Check for updates

European Journal of Inorganic Chemistry

EurJIC
European Journal of Inorganic Chemistry

Chemistry Europe
European Chemical Societies Publishing

RESEARCH ARTICLE OPEN ACCESS

Exploring the Anticancer Activity of Ruthenium(II)–Arene and Copper(I) Complexes Bearing *N*-Heterocyclic Carbene Ligands Containing Azido, Pyridinium, and Ethisterone-Derived Triazole Groups

Alessia Schiavo[1] | Chiara Tupini[2] | Nicola Demitri[3] | Ilaria Lampronti[2] | Thomas Scattolin[1]

[1]Dipartimento di Scienze Chimiche, Università degli Studi di Padova, Padova, Italy | [2]Dipartimento di Scienze della Vita e Biotecnologie, Università degli Studi di Ferrara, Ferrara, Italy | [3]Elettra–Sincrotrone Trieste, Trieste, Italy

Correspondence: Ilaria Lampronti (lmi@unife.it) | Thomas Scattolin (thomas.scattolin@unipd.it)

Received: 7 April 2026 | **Revised:** 10 June 2026 | **Accepted:** 8 July 2026

Keywords: anticancer activity | apoptosis | copper(I) complexes | *N*-heterocyclic carbenes | ruthenium(II) complexes

ABSTRACT

The design and functionalization of *N*-heterocyclic carbene (NHC) ligands provide a versatile platform for tuning the chemical and biological properties of metallodrugs. Herein, we report the synthesis of a series of backbone functionalized imidazolium precursors incorporating chloromethyl, azidomethyl, triazole–steroid, and pyridinium motifs, introduced to enable postfunctionalization, exploit the bioactive and bio-orthogonal properties of azides, confer potential hormone-receptor interactions through a steroidal fragment, and promote mitochondrial targeting through a lipophilic cationic unit, respectively, while maintaining steric protection around the metal binding site. These precursors were efficiently converted into Cu(I)–NHC complexes via a weak-base protocol and into Ru(II)–arene carbonato and dichloro NHC complexes using an analogous methodology, highlighting operationally simple, scalable approaches suitable for sensitive or multifunctional ligands. Structural characterization confirmed the formation of well-defined metal–carbene species. Biological evaluation revealed that Cu(I)–NHC complexes exhibit potent antiproliferative activity against ovarian (A2780, A2780cis) and breast (MCF-7) cancer cells, including cisplatin-resistant models, and induce apoptosis with moderate selectivity over nontumorigenic keratinocytes. In contrast, Ru(II)–NHC complexes displayed moderate cytotoxicity but are consistent with profiles favoring anti-metastatic and mechanistically distinct actions. These results underscore the potential of backbone-functionalized NHC ligands to fine-tune metallodrug activity and highlight Cu(I)–NHC complexes as promising candidates for further development against resistant cancers.

1 | Introduction

Cancer remains one of the leading causes of mortality worldwide, with breast and ovarian cancers representing two of the most prevalent and clinically challenging malignancies affecting women. Breast cancer is the most frequently diagnosed cancer in women and encompasses a heterogeneous group of diseases characterized by distinct molecular subtypes, including hormone-receptor–positive tumors such as those represented by the widely used MCF-7 human breast cancer cell line [1, 2]. The growth of these tumors is strongly influenced by estrogen signaling, and endocrine therapies targeting estrogen receptor pathways, including selective estrogen receptor modulators, aromatase inhibitors, and selective estrogen receptor degraders, constitute a cornerstone of treatment. Nevertheless, resistance to hormonal therapy and disease relapse remain major clinical challenges, highlighting the need for complementary therapeutic strategies.

This is an open access article under the terms of the Creative Commons Attribution License, which permits use, distribution and reproduction in any medium, provided the original work is properly cited.

© 2026 The Author(s). *European Journal of Inorganic Chemistry* published by Wiley-VCH GmbH.

Ovarian cancer, particularly high-grade serous ovarian carcinoma, remains one of the most lethal gynecological malignancies and is frequently diagnosed at advanced stages, resulting in poor long-term survival rates [3–5]. Although significant advances in surgical techniques and systemic therapies have improved patient management, disease relapse and limited long-term treatment efficacy remain common, underscoring the urgent need for new therapeutic strategies capable of overcoming resistance mechanisms and improving treatment selectivity.

Among alternative approaches, metal-based therapeutics have attracted sustained interest in medicinal chemistry. The clinical success of platinum drugs such as cisplatin, carboplatin, and oxaliplatin demonstrated the potential of metal complexes as powerful chemotherapeutic agents. These compounds exert their activity primarily through the formation of DNA crosslinks that interfere with replication and transcription, ultimately triggering apoptosis [6–9]. Despite their remarkable efficacy, platinum drugs suffer from important limitations, including severe side effects, acquired resistance, and limited selectivity for cancer cells [10]. To address these drawbacks, extensive research has explored platinum complexes in alternative oxidation states, including Pt(IV) prodrugs designed to improve pharmacokinetic properties and intracellular activation profiles [11, 12], less common Pt(0) systems [13, 14] as well as heterobimetallic complexes [15, 16]. Parallel efforts have focused on expanding the scope of metallodrugs beyond platinum, leading to the exploration of complexes based on metals such as ruthenium [17–21], gold [22–29], palladium [30–38] and copper [39–43]. These systems provide diverse coordination geometries, redox properties, and biological targets, enabling the development of compounds with mechanisms of action distinct from those of classical DNA-binding platinum agents.

Within this context, ruthenium complexes have emerged as promising candidates in anticancer drug discovery. Ruthenium possesses several features advantageous for medicinal applications, including accessible oxidation states, ligand exchange kinetics comparable to those of platinum, and the ability to mimic iron in certain biological processes [17–21]. Among ruthenium-based systems, half-sandwich Ru(II) arene complexes have been extensively investigated for their anticancer properties. This class of compounds typically adopts a "piano-stool" geometry, in which the η^6-arene ligand provides a stable platform while additional ligands modulate biological activity and pharmacological behavior [17–19]. Interestingly, several members of this family display relatively modest cytotoxicity toward primary tumor cells but pronounced activity in suppressing tumor invasion and metastasis, suggesting mechanisms of action that differ from conventional cytotoxic agents. Notable examples include phosphine-containing complexes such as those belonging to the RAPTA family (Ruthenium-Arene-PTA compounds), where the hydrophilic phosphine ligand PTA (1,3,5-triaza-7-phosphaadamantane) plays an important role in modulating solubility and biological activity [17–21]. While phosphine-based Ru(II) arene complexes have been widely studied, considerably less attention has been devoted to related systems incorporating *N*-heterocyclic carbene (NHC) ligands. Given the strong σ-donor character and tunable steric properties of NHCs [44–46], their incorporation into ruthenium arene frameworks represents an attractive strategy for modulating stability, reactivity, and biological behavior.

A second family of compounds investigated in the present study consists of copper(I) carbene complexes. Copper is an appealing metal for medicinal applications because it is an endogenous trace element involved in numerous biological processes, including redox regulation and enzymatic catalysis [47]. Most copper-based anticancer complexes reported in the literature involve Cu(II), largely due to the relative ease of stabilizing this oxidation state in aqueous and biological environments [39–42]. In contrast, Cu(I) complexes have been comparatively underexplored, despite their distinct coordination chemistry and potential biological activity. Interest in Cu(I) systems has been further stimulated by the recent discovery of cuproptosis, a newly identified form of regulated cell death driven by intracellular copper accumulation [48]. In this pathway, reduced copper species interact with lipoylated components of the tricarboxylic acid cycle, promoting protein aggregation and destabilization of iron–sulfur cluster proteins, ultimately leading to proteotoxic stress and cell death. These findings highlight the biological relevance of Cu(I) species and suggest that Cu(I)-containing complexes may represent valuable tools to exploit copper-dependent cytotoxic mechanisms in cancer cells. One effective strategy to stabilize Cu(I) centers involves the use of NHC ligands, which form strong σ-donor interactions and favor the formation of well-defined linear complexes. Recent studies have highlighted the potential of such systems in medicinal chemistry. In particular, a study by Scattolin, Nolan, and coworkers described a series of carbene–metal–amide (CMA) complexes incorporating carboline fragments that were evaluated for anticancer activity against several cancer models, including ovarian cancer tumoroids [43]. Interestingly, the copper derivatives in that series displayed higher cytotoxic activity than their silver and gold analogs, underscoring the potential of Cu(I)–NHC architectures as promising scaffolds for the development of novel anticancer agents.

Overall, NHCs have emerged as exceptionally versatile ligands in organometallic and medicinal chemistry. Their strong donor character, tunable steric properties, and ability to stabilize metals in multiple oxidation states have enabled the development of numerous NHC-containing complexes with significant biological activity [49, 50]. In the context of metallodrug design, NHC ligands confer high kinetic inertness to the metal center, protect complexes from rapid ligand exchange under physiological conditions, and allow systematic tuning of steric and electronic parameters.

In bioorganometallic chemistry, bulky *N*-substituted imidazol-2-ylidenes are commonly employed because their steric demand effectively shields the metal center from undesired ligand exchange and decomposition in biological environments. However, this steric protection often limits the introduction of additional functional groups that could promote interactions with biological targets. Traditional strategies to address this limitation have relied on modifying the *N*-substituents through pendant alkyl chains bearing polar or reactive groups [51, 52], although such modifications may reduce steric protection and compromise the kinetic stability of the resulting complexes.

10990682c, 0, Downloaded from https://chemistry-europe.onlinelibrary.wiley.com/doi/10.1002/ejic.70285 by Universita Di Ferrara, Wiley Online Library on [30/07/2026]. See the Terms and Conditions (https://onlinelibrary.wiley.com/terms-and-conditions) on Wiley Online Library for rules of use; OA articles are governed by the applicable Creative Commons License

An alternative strategy involves functionalizing the backbone of the NHC scaffold itself, thereby retaining bulky *N*-substituents while embedding functional groups directly within the carbene core. Backbone-modified NHCs can introduce hydrogen-bond donors or acceptors, redox-active motifs, or additional coordination sites, expanding the chemical space accessible to NHC-based metallodrugs. Until recently, however, this approach was limited by the synthetic accessibility of suitably functionalized NHC precursors [53, 54]. A significant advance was reported in 2022 by Ananikov and coworkers, who developed a mild and modular one-pot nucleophilic addition/cyclization protocol enabling the straightforward synthesis of heteroatom-functionalized azolium salts, greatly facilitating the preparation of backbone-functionalized NHC scaffolds [55].

Building on these advances, the present work exploits the possibility of selectively introducing a chloromethyl ($-CH_2Cl$) group within the NHC backbone. This functionality provides a convenient synthetic handle for postfunctionalization of the carbene precursor through nucleophilic substitution, enabling the incorporation of biologically relevant motifs while preserving the steric environment around the *N*-substituents. Using this strategy, we designed and synthesized a series of functionalized NHC ligands bearing three types of substituents with potential biological relevance.

First, azido groups were introduced as versatile functional moieties with well-documented biological and chemical properties. Organic azides are present in a variety of bioactive molecules and have found applications in medicinal chemistry as pharmacophores, bio-orthogonal handles, and precursors to nitrogen-containing heterocycles, with several azido-containing compounds displaying antimicrobial, antiviral, and anticancer activities [56, 57].

Second, the azide functionality was exploited as a handle for copper-catalyzed azide–alkyne cycloaddition (CuAAC), enabling the conjugation of the NHC scaffold to steroidal fragments [58]. In particular, we employed the terminal alkyne group of ethisterone to generate triazole-linked derivatives. Ethisterone (17α-ethynyltestosterone) is a synthetic steroid bearing a terminal alkynyl substituent at the C17 position, a structural modification that historically improved the metabolic stability and oral bioavailability of steroid hormones [59]. Introduced in the 1930s, ethisterone was one of the earliest orally active synthetic progestins and was widely used in hormonal therapy for menstrual disorders and endometriosis, as well as in early contraceptive formulations. Steroidal frameworks have attracted considerable attention as potential targeting vectors in cancer therapy because of their ability to interact with hormone receptors and steroid-binding proteins, a property particularly relevant in hormone-dependent tumors such as breast and ovarian cancers [60–62].

Finally, a pyridinium moiety was incorporated as a lipophilic cationic group capable of promoting mitochondrial targeting. Lipophilic cations such as pyridinium or triphenylphosphonium derivatives accumulate selectively within mitochondria due to the large negative membrane potential across the inner mitochondrial membrane, making them valuable tools for directing bioactive molecules toward mitochondrial targets [63].

In this work, we combine these ligand design principles with two complementary classes of metallodrugs—Ru(II) arene complexes and Cu(I)–NHC complexes—to investigate how backbone functionalization of NHC ligands influences the biological properties of the resulting metal complexes.

2 | Results and Discussion

2.1 | Synthesis of Backbone Functionalized Carbene Precursors

Following the synthetic strategy reported by Ananikov and coworkers for the preparation of substituted imidazolium salts from diazabutadienes through multicomponent reactions with orthoformates [55], we investigated this transformation on a larger preparative scale (15 g), focusing specifically on diazabutadienes bearing methyl substituents on the diene backbone.

Our study started from *N*,*N*′-bis(2,4,6-trimethylphenyl)−2,3-dimethyl-1,4-diaza-1,3-butadiene, a glyoxal-type diimine containing two methyl groups at the C2 and C3 positions of the backbone and two mesityl substituents on the nitrogen atoms. This compound was previously synthesized via condensation of 2,4,6-trimethylaniline (mesidine) with butane-2,3-dione (diacetyl), a well-established method for preparing sterically protected diazabutadienes [64]. The presence of bulky mesityl groups ensures sufficient stabilization of the diimine while maintaining good solubility and handling properties, making it a suitable substrate for further transformation.

The diazabutadiene was subsequently reacted with chlorotrimethylsilane (TMSCl) and triethyl orthoformate in ethyl acetate as solvent, deliberately using nonanhydrous conditions and performing the reaction under air for 24 h at room temperature (Scheme 1) [55]. Despite these relatively simple and nonstringent experimental conditions, the reaction proceeded cleanly and efficiently. During the course of the reaction, the desired product gradually precipitated from the reaction mixture as a white solid, allowing for a straightforward work-up. The compound was isolated by simple filtration, followed by washing with

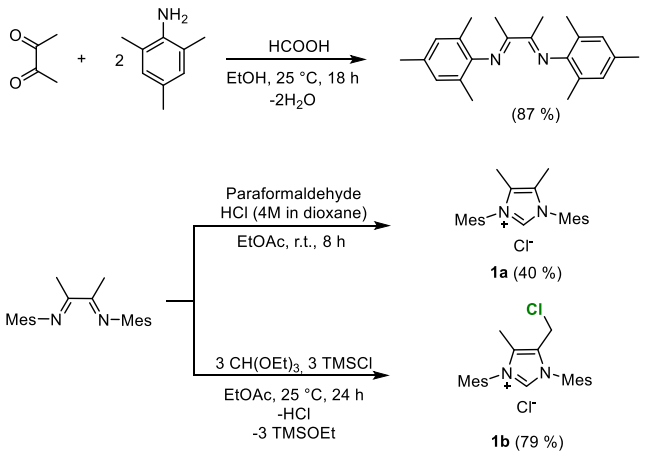

SCHEME 1 | Synthetic route to imidazolium salts **1a-b**.

10990682c, 0, Downloaded from https://chemistry-europe.onlinelibrary.wiley.com/doi/10.1002/ejic.70285 by Universita Di Ferrara, Wiley Online Library on [30/07/2026]. See the Terms and Conditions (https://onlinelibrary.wiley.com/terms-and-conditions) on Wiley Online Library for rules of use; OA articles are governed by the applicable Creative Commons License

small portions of ethyl acetate, affording the 4-chloromethyl-substituted imidazolium salt (**1b**) in high isolated yield (79%).

The formation of this product is fully consistent with the reactivity trends described in the work of Ananikov and colleagues for diazabutadienes containing methyl substituents in the backbone [55]. In the presence of triethyl orthoformate and TMSCl, these substrates undergo a multicomponent nucleophilic addition–cyclization process in which the diazabutadiene nitrogens attack the precarbenic carbon of the orthoformate, ultimately leading to formation of the imidazolium ring. Importantly, in methyl-substituted diazabutadienes the reaction pathway involves functionalization at the α-carbon of the backbone methyl group, which becomes the site of chloromethyl substitution, giving rise to the 4-chloromethyl imidazolium framework observed in compound **1b**.

In contrast, if the two methyl substituents were absent from the diazabutadiene backbone, the reaction would follow a different pathway. Unsubstituted glyoxal-derived diazabutadienes typically react with orthoformates to afford imidazolinium salts bearing two alkoxy substituents at the backbone positions. According to the mechanistic interpretation proposed in the original study, the absence of backbone substituents favors nucleophilic attack of alkoxy groups derived from the orthoformate at the electrophilic C2 and C3 positions of the diazabutadiene. However, when methyl groups are present, the reaction is diverted toward α-functionalization of the methyl substituent, enabling incorporation of chloride and ultimately leading to the formation of 4-chloromethyl-substituted imidazolium salts instead of the dialkoxy imidazolinium products.

Therefore, the presence of the two methyl groups in the diazabutadiene backbone plays a decisive role in controlling the reaction outcome, steering the multicomponent cyclization toward the chloromethylated imidazolium product and enabling an efficient and operationally simple synthesis of compound **1b** on multigram scale.

For comparison, the nonfunctionalized imidazolium analog (**1a**), which still contains the two methyl groups in the backbone but lacks further functionalization, was prepared through a different and more conventional cyclization protocol (Scheme 1) [65]. In this case, *N*,*N*′-bis(2,4,6-trimethylphenyl)−2,3-dimethyl-1,4-diaza-1,3-butadiene was reacted with paraformaldehyde in the presence of hydrochloric acid in dioxane, leading to cyclization and formation of the corresponding imidazolium salt (**1a**).

This nonfunctionalized imidazolium salt **1a**, together with its corresponding metal complexes described in this work, was used as a reference system. In particular, these compounds serve as benchmark standards to evaluate whether the biological activity of the different families of ruthenium(II)–arene and copper(I) complexes investigated in this study is influenced by the various functionalizations introduced on the imidazolium scaffold. By comparing the activity of the functionalized derivatives with that of the parent, nonfunctionalized system, it is possible to assess the role of backbone modification and pendant groups in modulating the biological properties of the resulting metal complexes.

The introduction of the azide functionality on the imidazolium scaffold was achieved through a simple nucleophilic substitution starting from the 4-chloromethyl-substituted imidazolium precursor (**1b**). Specifically, compound **1b** was treated with sodium azide (3 equiv.) in acetone at room temperature for 4 h. Under these mild conditions, the reaction proceeds affording the corresponding azidomethyl-functionalized imidazolium salt **1c**′ (Scheme 2).

During the reaction, the formation of a white precipitate of NaCl was clearly observed. This inorganic salt arises both from nucleophilic substitution of the chloromethyl group by azide and from anion exchange at the imidazolium center, whereby the chloride counterion of the starting salt is replaced by azide. Since NaCl is insoluble in acetone, it gradually precipitates from the reaction medium. After completion of the reaction, the inorganic salt was simply removed by filtration, and the solvent was evaporated under reduced pressure to afford compound **1c**′. The reaction proved readily scalable and was performed on a 5 g scale without any noticeable decrease in efficiency.

Although compound **1c**′ could be directly isolated in this way, an additional consideration was required for its use in the subsequent coordination chemistry explored in this work. In particular, the synthesis of the metal complexes described herein was carried out using the weak-base route, a widely employed strategy in NHC chemistry in which the imidazolium salt is converted in situ into the corresponding metal–NHC complex in a single step [66, 67].

In this context, the nature of the counterion of the imidazolium salt becomes particularly important. In compound **1c**′, the azide anion is present as the counterion and could potentially interfere with the coordination sphere of the metal precursor during the metalation step. Specifically, azide is capable of coordinating to transition metals and may therefore partially or completely replace anionic ligands (e.g., chlorides) originally bound to the metal precursor. Such ligand substitution processes could lead to undesired variations in the primary coordination sphere of the metal center, complicating the formation of the target carbene complexes and reducing synthetic control over the final structures.

To avoid these potential complications and maintain full control over the anion composition of the metal coordination sphere, an anion exchange was therefore performed to convert the azide salt

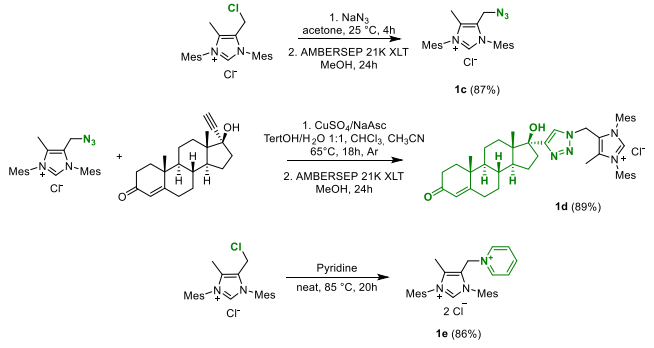

SCHEME 2 | Synthetic route to imidazolium salts **1c–e**.

10990682c, 0, Downloaded from https://chemistry-europe.onlinelibrary.wiley.com/doi/10.1002/ejic.70285 by Universita Di Ferrara, Wiley Online Library on [30/07/2026]. See the Terms and Conditions (https://onlinelibrary.wiley.com/terms-and-conditions) on Wiley Online Library for rules of use; OA articles are governed by the applicable Creative Commons License

1c′ into the corresponding imidazolium chloride (**1c**). This transformation was conveniently achieved using the chloride-form anion-exchange resin AMBERSEP 21K XLT.

The resulting azidomethyl-functionalized imidazolium chloride (**1c**) was characterized by NMR spectroscopy. Importantly, the ^{1}H NMR spectrum of compound **1c** retains all the characteristic signals observed for the parent chloromethyl precursor (**1b**). However, a diagnostic shift is observed for the methylene protons of the functionalized side chain. In particular, the CH_2 group originally bound to chlorine in compound **1b**, which appears at 4.8 ppm (CH_2Cl), shifts upfield to approximately 4.3 ppm after substitution with the azide group. Additionally, a noticeable shift is observed for the acidic imidazolium proton (NCHN), whose resonance moves from 9.6 ppm in the chloromethyl precursor to 10.9 ppm in compound **1c**.

The fourth imidazolium salt prepared in this preliminary phase is an unprecedented azide–alkyne conjugate, obtained by exploiting the well-established reactivity of the azide group toward terminal alkynes, that is, a Cu(I)-catalyzed azide–alkyne cycloaddition ("click" reaction). For this transformation, the terminal alkyne was chosen to be ethisterone, a biologically relevant steroid known for its hormonal activity and widespread use in gynecological applications. This choice allows investigation of the potential of bioconjugation to enhance antitumor activity.

Following precedent in the literature, in which ethisterone was coupled to a different azide scaffold [68], the reaction was carried out between compound **1c** (azidomethyl-functionalized imidazolium chloride) and ethisterone in a 1:1 stoichiometric ratio, using $CuSO_4$ as the copper source and sodium ascorbate as a reducing agent to generate the catalytically active Cu(I) species in situ. To ensure effective solubilization of all reaction components, a quaternary solvent mixture of *tert*-butanol, water, chloroform, and acetonitrile was employed. In this system, *tert*-butanol serves as a phase-transfer mediator, facilitating the interaction between the aqueous Cu(I) catalyst and the organic substrates. The reaction was conducted at 65 °C under argon for 18 h to prevent oxidation of the Cu(I) species.

After completion, the reaction mixture was subjected to a simple chloroform/water extraction, removing inorganic salts and water-soluble byproducts. The organic phase was dried over $MgSO_4$, and the solvent was removed under reduced pressure. Given the presence of multiple anions in solution (ascorbate, sulfate, chloride), the nature of the counterion of the resulting imidazolium salt was not guaranteed. Therefore, an anion exchange using AMBERSEP 21K XLT chloride-form resin was performed, yielding the azide–alkyne conjugated imidazolium chloride (**1d**) on a gram scale with an overall yield of 89%.

The structure of **1d** was confirmed by ^{1}H NMR spectroscopy. Comparison with the spectra of the precursor **1c** and free ethisterone shows clear evidence of conjugation. The acidic imidazolium proton (NCHN) shifts from approximately 11 ppm in compound **1c** to 9.5 ppm in **1d**, and resonances associated with the methylene protons of the imidazolium backbone shift from 4.5 to 5.5 ppm, consistent with the transformation of the azide precursor. Signals corresponding to the steroid fragment display general shifts of the aliphatic protons, with the disappearance of the terminal alkyne proton at 2.5 ppm and the appearance of the characteristic 1,2,3-triazole proton at ca. 6 ppm. Additionally, the enolic proton of the steroid moiety resonates at 5.6 ppm.

In the ^{13}C NMR spectrum, the methylene carbon adjacent to the triazole resonates at 42 ppm, the triazole CH at 123.5 ppm, and the steroidal enolic carbon at 123.8 ppm. The carbonyl carbon of the steroid fragment appears at 199.5 ppm, while the imidazolium C2 carbon (NCHN) is observed at 135 ppm.

The final imidazolium salt prepared in this study (**1e**) was obtained by introducing a CH_2-pyridinium moiety onto the 4-chloromethyl-substituted imidazolium precursor (**1b**). To achieve this transformation, compound **1b** was dissolved in pyridine, which served simultaneously as solvent and nucleophilic reagent. The reaction mixture was stirred at 85 °C for 20 h, after which the desired pyridinium-functionalized imidazolium salt was isolated by simple filtration and washed with diethyl ether. The reaction was performed on a gram scale and afforded the product in high yield (86%).

The structure of **1e** was confirmed by ^{1}H NMR spectroscopy. The aliphatic region (δ = 1.7–2.5 ppm) shows the methylene and methyl signals of the imidazolium backbone and mesityl groups. The methylene protons (CH_2–Py^+) appears at δ = 5.9 ppm, approximately 1 ppm downfield relative to the corresponding signal in precursor **1b**, consistent with the electron-withdrawing effect of the positively charged pyridinium group. Aromatic signals of the mesityl groups appear between δ = 7–7.5 ppm, while the diagnostic pyridinium protons are observed at δ = 8–8.5 ppm, significantly downfield relative to free pyridine, reflecting the formal positive charge on the pyridinium nitrogen.

The spectral data are fully consistent with literature reports for this compound [55], confirming successful installation of the CH_2–pyridinium group onto the imidazolium scaffold.

2.2 | Synthesis of Copper(I)–NHC Complexes

The target copper complexes were designed as linear Cu(I)–NHC species of general formula [NHC–Cu–Cl], a well-established structural motif in copper(I) carbene chemistry. Two main synthetic approaches are typically employed for the preparation of such complexes: the built-in base route and the weak-base route.

The built-in base route relies on the use of Cu_2O as both metal source and internal base, promoting deprotonation of the imidazolium salt and formation of the Cu(I)–NHC complex through a direct acid–base reaction that generates water as the byproduct [69]. However, this method usually requires anhydrous organic solvents (e.g., dichloromethane or toluene) and strictly controlled conditions, as the presence of moisture may compromise the stability of Cu_2O and shift the equilibrium toward the starting materials. In addition, the higher reactivity of copper(I) relative to silver(I) often leads to lower reproducibility and competing redox processes, making this approach less reliable for routine synthesis.

For these reasons, the weak-base route, originally reported by Nolan and coworkers and later applied to Cu(I)–NHC systems by Cazin [70], was selected as the synthetic strategy in this work.

10990682c, 0, Downloaded from https://chemistry-europe.onlinelibrary.wiley.com/doi/10.1002/ejic.70285 by Universita Di Ferrara, Wiley Online Library on [30/07/2026]. See the Terms and Conditions (https://onlinelibrary.wiley.com/terms-and-conditions) on Wiley Online Library for rules of use; OA articles are governed by the applicable Creative Commons License

This method involves the reaction of an imidazolium salt with CuCl in the presence of a weak and inexpensive inorganic base such as K_2CO_3 in acetone at moderate temperature (60 °C). Under these conditions, the imidazolium salt initially interacts with CuCl to form a cuprate intermediate of general formula $[CuCl_2]^-$ paired with the imidazolium cation. This intermediate increases the acidity of the C2–H proton, facilitating its deprotonation by the weak base. The resulting NHC is then generated in situ and immediately coordinates to the copper center, affording the desired Cu(I)–NHC complex in a single step. The methodology is operationally simple, does not require an inert atmosphere or rigorously anhydrous solvents, and generates only inorganic salts as byproducts, thus offering good atom economy and synthetic practicality.

Using this approach, the target Cu(I)–NHC complexes were prepared starting from the five imidazolium salts (**1a–e**) described in the previous section. Specifically, the imidazolium salt was reacted with CuCl in the presence of K_2CO_3 in technical acetone at 60 °C for 18 h (Scheme 3). After completion, the solvent was removed under reduced pressure, and the crude residue was dissolved in a minimal amount of dichloromethane. Inorganic salts and traces of unreacted imidazolium salt were removed by filtration through a short silica plug, and the complexes were isolated after solvent removal, generally in high yields and purity.

While this protocol proved effective for most of the imidazolium salts investigated, a notable exception was observed for the pyridinium-functionalized precursor (**1e**). Under the standard reaction conditions, the mixture rapidly developed a black precipitate, and the isolated material exhibited complex ^{1}H NMR spectra consistent with decomposition products rather than the desired Cu–NHC complex. To better understand this behavior, the reaction between **1e** and CuCl was also examined in the absence of base. In this case, the formation of a poorly soluble cuprate species was observed, suggesting that precipitation of this intermediate may inhibit efficient carbene generation. The reaction therefore likely proceeds under heterogeneous conditions, where the limited solubility of the cuprate intermediate prevents productive deprotonation and favors competing decomposition pathways.

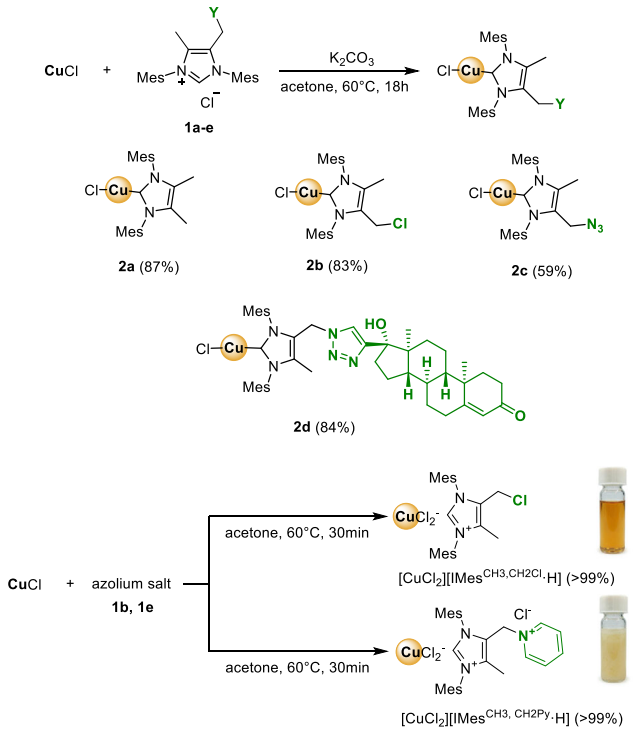

SCHEME 3 | Synthetic route to Cu(I)–NHC complexes and their cuprate intermediates.

Attempts to obtain the corresponding complex **2e** using the built-in base route with Cu_2O in dichloromethane were also explored. However, even after extended reaction times of several days, this approach did not lead to selective formation of the desired complex, further highlighting the limited compatibility of the pyridinium-functionalized ligand with these metalation conditions.

In contrast to the behavior observed for the pyridinium-functionalized precursor, the cuprate intermediates formed from the other imidazolium salts (**1a–d**) upon reaction with CuCl in the absence of base were found to be fully soluble in the reaction medium and, therefore readily available for the subsequent base-assisted metalation step with K_2CO_3.

To support this mechanistic picture, the interaction between imidazolium salt **1b** and CuCl was examined under base-free conditions. Upon heating in acetone, CuCl gradually dissolved, yielding a homogeneous brown solution. Removal of the solvent afforded a species that, according to ^{1}H NMR spectroscopy, displays noticeable chemical shift variations compared to the starting imidazolium salt, particularly for the NCHN proton, consistent with the formation of a new ionic species (**[CuCl$_2$][IMes^{CH3,CH2Cl}·H]**).

Definitive structural information was obtained by single-crystal X-ray diffraction, which revealed the presence of a cuprate ion pair of general formula $[CuCl_2]^-$ associated with the imidazolium cation (Figure 1).

This observation provides direct experimental evidence for the involvement of soluble cuprate intermediates in the weak-base pathway, which likely facilitate the subsequent deprotonation of the imidazolium C2–H and formation of the Cu(I)–NHC complex.

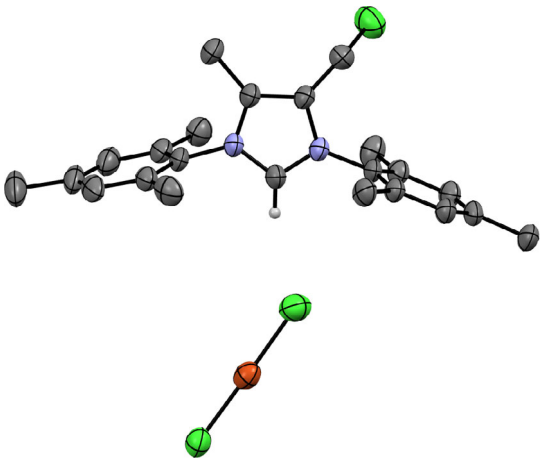

FIGURE 1 | X-ray molecular structure of the cuprate intermediate **[CuCl$_2$][IMes^{CH3,CH2Cl}·H]** is presented, with nonrelevant hydrogen atoms omitted for clarity (blue = N, gray = C, red = Cu, and green = Cl).

10990682c, 0, Downloaded from https://chemistry-europe.onlinelibrary.wiley.com/doi/10.1002/ejic.70285 by Universita Di Ferrara, Wiley Online Library on [30/07/2026]. See the Terms and Conditions (https://onlinelibrary.wiley.com/terms-and-conditions) on Wiley Online Library for rules of use; OA articles are governed by the applicable Creative Commons License

The Cu(I)–NHC complexes successfully obtained from the imidazolium salts **1a–d** were characterized by ^{1}H and ^{13}C NMR spectroscopy. In the ^{1}H NMR spectra, the signals associated with the imidazolium precursors are largely retained but generally appear slightly shifted upfield, consistent with increased shielding induced by coordination to the copper center. Importantly, the diagnostic acidic imidazolium proton (NCHN) present in the starting salts disappears upon complex formation, indicating successful carbene generation. Further confirmation was obtained from the ^{13}C NMR spectra, where the appearance of a resonance in the region 175–180 ppm is attributed to the carbene carbon coordinated to copper, a characteristic signature of Cu(I)–NHC complexes.

2.3 | Synthesis of [Ru(η⁶-*p*-Cymene)(NHC)(CO_3)] Complexes

The interest in Ru(II)–arene complexes as anticancer agents has increased significantly in recent years, particularly following the promising biological activity reported for the RAPTA complexes family, which display enhanced activity toward metastatic tumors compared with primary tumors [17–21]. In this context, replacing the phosphine ligand (PTA) with an *N*-heterocyclic carbene represents an attractive strategy to combine the biological relevance of Ru(II)–arene scaffolds with the strong σ-donor properties and tunability of NHC ligands.

Several synthetic approaches are available for the preparation of Ru–NHC complexes [66]. Generation of the free carbene through deprotonation of the imidazolium salt with strong bases followed by coordination to the metal precursor is commonly employed but requires strictly inert conditions and shows limited tolerance toward functional groups bearing acidic protons. Alternatively, transmetalation from Ag(I)–NHC complexes can be used, although this approach introduces additional synthetic steps, increases costs, and requires careful exclusion of light due to the photosensitivity of silver carbene complexes. Moreover, residual silver salts may interfere with subsequent biological studies.

For these reasons, the weak-base route was selected as the synthetic strategy. This methodology, recently applied to Ru(II)–arene systems by Nolan and coworkers, involves the direct reaction of the imidazolium salt, K_2CO_3, and the dimeric precursor [Ru(*p*-cymene)Cl_2]$_2$ in acetone at 60 °C [71]. In contrast to other metals commonly investigated in medicinal inorganic chemistry, Ru(II) tends to adopt an octahedral coordination environment, which allows the carbonate anion to play a dual role as both base and chelating ligand. As a result, the products of the reaction are carbonato Ru(II)–NHC complexes.

The weak-base protocol was first validated using the nonfunctionalized imidazolium salt **1a**, confirming that complete conversion is achieved after approximately 18 h (Scheme 4).

After removal of the solvent, the crude mixture was filtered through a PTFE membrane to remove inorganic salts, as the complexes proved unstable toward silica. The residue was then dissolved in dichloromethane and triturated with diethyl ether to afford the desired Ru–NHC complex in good yield. The same procedure was subsequently extended to the other imidazolium salts (**1b–e**).

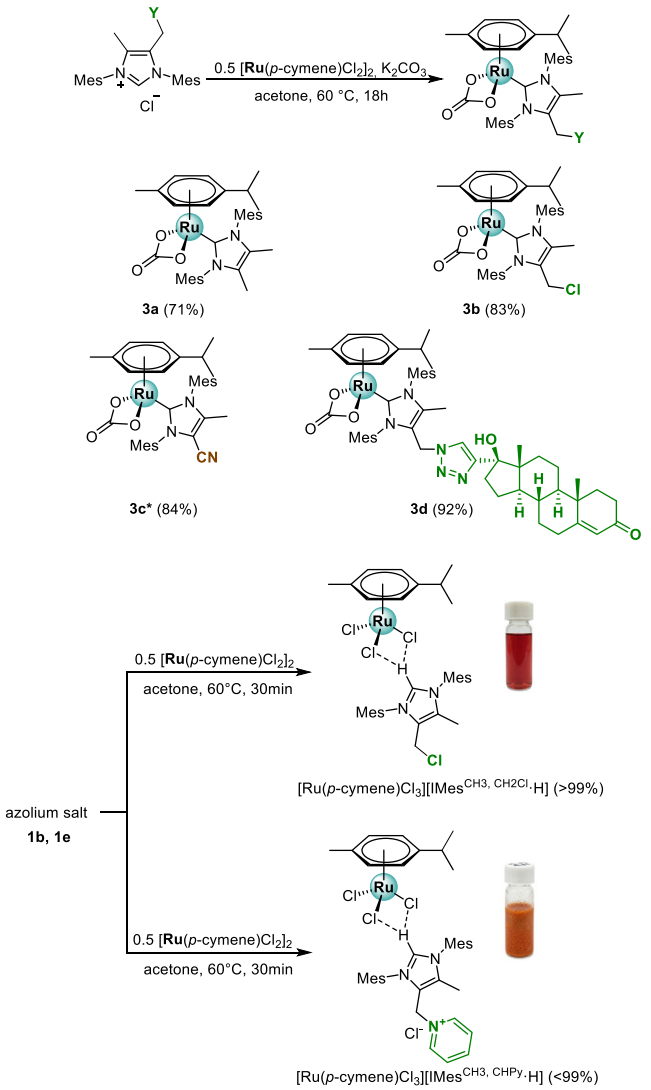

SCHEME 4 | Synthetic route to [Ru(η⁶-*p*-cymene)(NHC)(CO_3)] complexes and their rutenate intermediates.

Similarly to what was observed for the Cu(I) system, the pyridinium-functionalized precursor **1e** did not yield the corresponding Ru–NHC complex. When the reaction was attempted under standard weak-base conditions, precipitation of a dark solid was observed, and the isolated material showed NMR features consistent with decomposition. Additional experiments conducted in the absence of base indicated the formation of a poorly soluble intermediate species arising from the interaction between the imidazolium salt and the Ru(II) precursor. In contrast, reactions performed with the other imidazolium salts produced clear solutions, consistent with the formation of soluble ruthenate ion pairs, plausibly formulated as [$RuCl_3$(*p*-cymene)]$^-$ associated with the imidazolium cation. The low solubility of the intermediate generated from the pyridinium salt, combined with the dicationic nature of the ligand framework, likely prevents efficient carbene generation and ultimately hampers complex formation.

The obtained Ru(II)–NHC carbonato complexes were characterized by ^{1}H and ^{13}C NMR spectroscopy. In the ^{1}H NMR spectra, the most diagnostic feature is the complete disappearance of the imidazolium NCHN proton, indicating successful carbene

10990682c, 0, Downloaded from https://chemistry-europe.onlinelibrary.wiley.com/doi/10.1002/ejic.70285 by Universita Di Ferrara, Wiley Online Library on [30/07/2026]. See the Terms and Conditions (https://onlinelibrary.wiley.com/terms-and-conditions) on Wiley Online Library for rules of use; OA articles are governed by the applicable Creative Commons License

formation. In addition, the signals corresponding to the coordinated *p*-cymene ligand display the characteristic pattern expected for η^6-arene Ru(II) complexes. The aliphatic region contains resonances attributable both to the carbene ligand and to the isopropyl and methyl groups of *p*-cymene, while the aromatic protons of the arene appear significantly upfield-shifted (4.5–5.5 ppm) due to shielding effects induced by metal coordination.

Analysis of the ^{13}C NMR spectra further confirms complex formation. In all cases, a resonance corresponding to the Ru-bound carbene carbon appears at ca. 180 ppm, while a second diagnostic signal at ca. 166 ppm is attributed to the coordinated carbonate ligand. The arene carbons of *p*-cymene resonate in the 90–100 ppm region, consistent with η^6-coordination to an electron-rich metal center.

Two systems displayed distinctive behavior. In the case of the complex derived from the azide-functionalized ligand, the expected azidomethyl resonance was absent in the ^1H NMR spectrum, indicating modification of the functional group during the reaction. Single-crystal X-ray diffraction analysis revealed that the ligand had undergone conversion of the azide moiety into a nitrile group, while the Ru(II) center retained the expected *p*-cymene and carbonato ligands (see Figure 2 of complex **3c***). Unfortunately, only a small fraction of this compound could be isolated in sufficiently pure form after multiple recrystallizations, yielding enough material for crystal growth suitable for XRD analysis. The overall amount of pure product was too low to perform further transformations, such as the carbonato-to-dichloro exchange described in the following section, or to conduct biological studies.

This transformation can plausibly be rationalized by Ru-mediated redox processes, involving initial reduction of the azide to an amine followed by oxidation to the corresponding nitrile. Such reactivity is consistent with the well-known redox flexibility of Ru(II)/Ru(III) systems and with the catalytic activity of Ru–arene complexes in amine oxidation reactions [72].

A second unusual case was observed for the triazole–ethisterone conjugated complex, whose ^1H and ^{13}C NMR spectra revealed the presence of two closely related species displaying identical sets of signals with slight chemical-shift differences. Due to the limited thermal stability of this compound in common deuterated solvents, variable-temperature NMR experiments could not be performed. However, based on precedents reported for bulky metal–NHC complexes, these two species are tentatively assigned to atropoisomers, arising from restricted rotation around the Ru—C(carbene) bond caused by the steric demand and asymmetry introduced by the steroidal substituent. Consistent with this interpretation, ligands lacking such steric bulk give rise to a single observable species in solution.

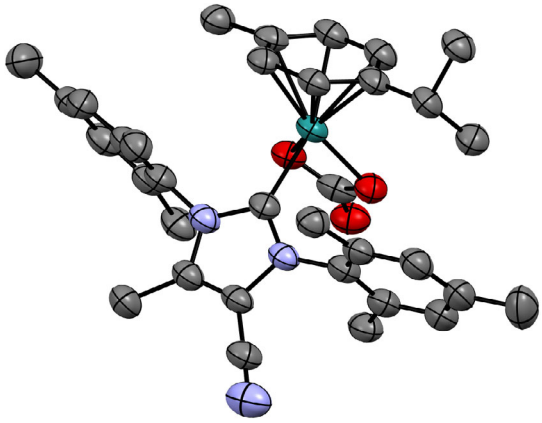

FIGURE 2 | X-ray molecular structure of the Ru(II)-NHC complex **3c*** is presented, with hydrogen atoms omitted for clarity (blue = N, gray = C, red = O, green = Ru).

2.4 | Synthesis of [Ru(η^6-*p*-Cymene)(NHC)Cl_2] Complexes

Following the preparation of the Ru(II)–NHC carbonato complexes, the corresponding dichloro derivatives were obtained in order to evaluate the influence of ancillary ligands on the properties of the metal center. The transformation was performed according to the protocol reported by Nolan and coworkers [71].

In practice, the Ru(II)–NHC carbonato complexes **3a–d** were treated with 3 equiv. of trimethylsilyl chloride (TMSCl) in THF at room temperature. Under these conditions, rapid substitution of the coordinated carbonate occurs, affording the corresponding dichloro Ru(II)–NHC complexes **4a, 4b**, and **4d** within a few minutes (Scheme 5).

The products were isolated by simple precipitation from THF with diethyl ether, providing the expected compounds in quantitative yields.

The resulting complexes were characterized by ^1H and ^{13}C NMR spectroscopy. The ^1H NMR spectra largely retain the signal pattern observed for the corresponding carbonato species, reflecting the similar coordination environment around the Ru(II) center, although small chemical-shift variations are observed. The most diagnostic evidence for carbonate substitution is provided by the ^{13}C NMR spectra, where the resonance previously attributed to the coordinated carbonate carbon ($\delta \approx 166$ ppm) completely disappears in the dichloro derivatives.

As observed for the corresponding carbonato complex, the compound bearing the triazole–ethisterone substituent displays two sets of NMR signals in both ^1H and ^{13}C spectra, corresponding to a mixture of atropoisomeric species.

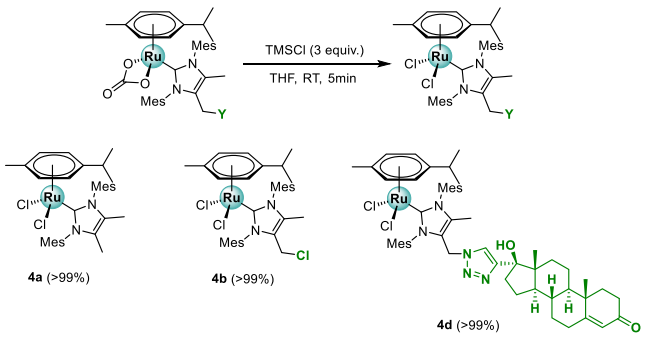

SCHEME 5 | Synthetic route to [Ru(η^6-*p*-cymene)(NHC)Cl_2] complexes.

10990682c, 0, Downloaded from https://chemistry-europe.onlinelibrary.wiley.com/doi/10.1002/ejic.70285 by Universita Di Ferrara, Wiley Online Library on [30/07/2026]. See the Terms and Conditions (https://onlinelibrary.wiley.com/terms-and-conditions) on Wiley Online Library for rules of use; OA articles are governed by the applicable Creative Commons License

Because the pyridinium-functionalized ligand did not yield the corresponding Ru–NHC complex **3e** under weak-base conditions, the dichloro derivative **4e** was instead accessed through a transmetalation strategy (Scheme 6).

In this case, the corresponding Ag(I)–NHC complex **5e** was first generated by reacting the imidazolium salt with Ag_2O in dichloromethane under an argon atmosphere. After approximately 16 h, complete consumption of the starting imidazolium salt was observed. The resulting silver complex **5e** shows the expected NMR features, including the absence of the diagnostic NCHN proton, consistent with carbene formation.

Subsequent reaction of this Ag(I)–NHC complex with the dimeric Ru(II) precursor led to rapid formation of the target Ru(II)–NHC dichloro complex **4e**, accompanied by immediate precipitation of AgCl. After filtration through a PTFE membrane to remove the silver salt, the product was isolated by precipitation from a diethyl ether/pentane mixture. The ^{1}H NMR spectrum confirms the disappearance of the signals associated with the Ag(I) precursor and the appearance of the characteristic resonances of the Ru–NHC complex.

Similarly to the triazole–ethisterone derivative, the pyridinium–containing complex displays two closely related sets of NMR signals, indicating the presence of atropoisomeric species. This behavior is consistent with the increased steric congestion generated by the bulky and asymmetric substituent appended to the NHC backbone, which restricts rotation around the Ru—C(carbene) bond.

2.5 | Antiproliferative Activity on Ovarian Cancer, Breast Cancer, and Noncancerous Cells

The antiproliferative activity of the synthesized complexes was evaluated in order to assess the influence of both the metal center and the NHC ligand functionalization on their biological profile. The study included the series of Cu(I)–NHC complexes (**2a–d**), the corresponding Ru(II)–NHC dichloro derivatives (**4a**, **4b**, and **4d–e**), and two representative Ru(II) carbonato complexes (**3b** and **3d**).

Antiproliferative activity was investigated against human cancer cell lines representative of ovarian and breast tumors, namely A2780 ovarian carcinoma, its cisplatin-resistant counterpart A2780*cis*, and MCF-7 breast adenocarcinoma. In addition, the immortalized keratinocyte HaCaT line was included as a nontumoral model to evaluate possible selectivity toward malignant cells. The biological response was quantified through determination of the IC_{50} value.

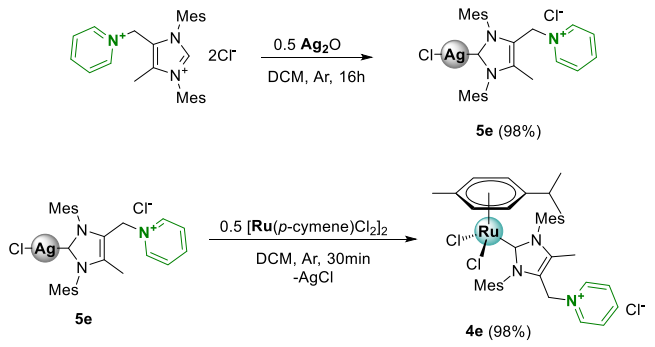

SCHEME 6 | Synthesis of complex **4e** via transmetalation.

Stock solutions of the complexes were prepared in sterile dimethylformamide (DMF) and subsequently diluted in the cell culture medium. Preliminary ^{1}H NMR stability studies indicated that the complexes remain stable in d_7-DMF and in d_7-DMF/D_2O mixtures over the time scale relevant to the biological assays (24 h). Consistently, UV–Vis studies under biologically relevant conditions revealed an essentially unchanged spectral profile over 72 h, with only a minor decrease in absorbance intensity likely due to partial precipitation. By contrast, the commonly used solvent dimethyl sulfoxide (DMSO) induced decomposition of the complexes, likely due to its strong coordinating ability, and was therefore avoided. Control experiments confirmed that DMF itself shows negligible cytotoxicity under the conditions employed, with cell viability values remaining between 95% and 98%. For comparison, treatments with the reference drug cisplatin were also performed to provide a benchmark for evaluating the activity of the synthesized compounds.

The antiproliferative activity was first evaluated on A2780 ovarian carcinoma cells and on the cisplatin-resistant A2780*cis* line (Table 1). The latter provides an important model for assessing whether new compounds can overcome resistance mechanisms typically associated with platinum drugs.

Across both ovarian cell lines, a clear trend emerged. The Cu(I)–NHC complexes (**2a–d**) consistently exhibited the highest antiproliferative activity, with IC_{50} values comparable to or lower than those measured for cisplatin. In particular, the nonfunctionalized complex **2a** proved to be the most active compound of the series, while the triazole–steroid conjugate **2d** showed slightly reduced activity. Overall, however, all copper complexes displayed IC_{50} values within the same order of magnitude, suggesting that backbone functionalization has only a modest influence on cytotoxic potency within this family.

A particularly notable result is the retention of activity in the cisplatin-resistant A2780*cis* cells. While cisplatin displays a dramatic loss of efficacy in this model, the Cu(I) complexes maintain essentially the same potency observed in the sensitive line. This behavior strongly suggests that these compounds operate through a mechanism of action distinct from that of Pt(II) drugs, allowing them to bypass typical resistance pathways.

In contrast, the Ru(II)–NHC complexes (**4a–b**, **4d–e**, **3b,** and **3d**). displayed moderate antiproliferative activity, with IC_{50} values generally ranging between 25 and 50 μM. Only minor differences were observed between the carbonate and dichloro derivatives, indicating that substitution of the carbonate ligand by chloride has limited influence on cytotoxicity in this system. This range of IC_{50} values suggests that these Ru(II) complexes are approximately ten times less active than cisplatin in the cisplatin-sensitive ovarian cell line but exhibit comparable activity to cisplatin in the cisplatin-resistant one, consistent with a mechanism of action distinct from Pt(II)-based chemotherapy. Overall, their potency remains significantly lower than that of the Cu(I)–NHC analogs (**2a–d**), which retain high activity across both sensitive and resistant cell lines.

10990682c, 0, Downloaded from https://chemistry-europe.onlinelibrary.wiley.com/doi/10.1002/ejic.70285 by Universita Di Ferrara, Wiley Online Library on [30/07/2026]. See the Terms and Conditions (https://onlinelibrary.wiley.com/terms-and-conditions) on Wiley Online Library for rules of use; OA articles are governed by the applicable Creative Commons License

TABLE 1 | IC_{50} (μM) of the newly synthesized Cu(I)–NHC and Ru(II)–NHC complexes and cisplatin on ovarian cancer (A2780, A2780*cis*), breast cancer (MCF-7) and noncancerous (HaCaT) cell lines.

	IC_{50} (μM)				
Complex	**A2780**	**A2780*cis***	**MCF-7**	**HaCaT**	**S.I.**
Cisplatin	**1.9 ± 0.3**	**25.2 ± 0.7**	**20 ± 7**	**13 ± 2**	**0.8**
2a	0.35 ± 0.01	0.13 ± 0.03	0.45 ± 0.01	2.7 ± 0.1	8.7
2b	0.62 ± 0.08	0.6 ± 0.3	3.0 ± 0.9	1.54 ± 0.08	1.1
2c	0.45 ± 0.07	0.26 ± 0.01	0.69 ± 0.02	2.1 ± 0.3	4.5
2d	0.88 ± 0.04	1.8 ± 0.2	2.9 ± 0.6	2.8 ± 0.1	1.5
3b	52 ± 5	>100	41 ± 5	54 ± 6	<0.8
3d	44.5 ± 0.8	24 ± 10	23 ± 2	25 ± 1	0.67
4a	40 ± 5	29 ± 8	42.0 ± 0.8	31 ± 5	0.8
4b	49 ± 4	27 ± 12	41 ± 3	42 ± 2	1.1
4d	42.9 ± 0.4	45 ± 6	92 ± 2	21.1 ± 0.1	0.4
4e	40 ± 18	34 ± 6	5 ± 3	57 ± 6	2.2

Note: Complexes were initially dissolved in DMF to obtain 50 mM stock solutions, which were then diluted with water and cell culture medium to achieve the concentrations required for IC_{50} determination. Bold is used for complexes name, cell lines and IC50 of reference drug (cisplatin).

Evaluation on MCF-7 breast adenocarcinoma cells revealed a trend closely resembling that observed for the ovarian models. The Cu(I)–NHC complexes (**2a–d**) again represent the most active class, with IC_{50} values frequently lower than that of cisplatin. The same structure–activity pattern is observed, with **2a** remaining the most potent compound and the steroid–derived complex **2d** showing comparatively lower activity.

The Ru(II) complexes display again moderate cytotoxicity, with IC_{50} values around ∼50 μM and only minor variations across the ligand series. These results are broadly consistent with previous reports indicating that Ru(II)–arene complexes often show limited activity toward primary tumor models, while their therapeutic potential may instead be related to anti-metastatic or anti-angiogenic effects.

The activity of the complexes toward HaCaT keratinocytes was examined to assess their potential selectivity toward malignant cells. The Cu(I) complexes **2a–d**, despite their strong antiproliferative activity, also display relatively low IC_{50} values in the nontumoral line, indicating limited intrinsic selectivity. To quantify this aspect, the selectivity index (SI) was calculated as the ratio between the IC_{50} measured for HaCaT cells and the average IC_{50} obtained across the tumor cell lines. In medicinal chemistry, SI values greater than 10 are generally considered indicative of strong selectivity toward cancer cells.

Within the copper series, the highest selectivity indexes were observed for complexes **2a** and **2c** (8.7 and 4.5, respectively). Although these values are below the threshold generally considered indicative of highly selective agents (SI > 10), they still reflect a moderate and meaningful degree of selectivity toward tumor cells over nontumor cells. By contrast, the Ru(II) complexes and cisplatin show SI values close to unity, indicating comparable activity toward both tumor and nontumor cells. Among the ruthenium derivatives, the pyridinium–functionalized complex **4e** displays the most favorable selectivity profile, albeit combined with only moderate cytotoxic potency.

Taken together, the biological data highlight clear differences between the two metal platforms investigated. The Cu(I)–NHC complexes emerge as the most promising candidates, combining strong antiproliferative activity with the ability to retain efficacy in cisplatin-resistant ovarian cancer cells. In particular, complexes **2a** and **2c** provide the best overall balance between potency and selectivity.

Conversely, the Ru(II)–NHC complexes display moderate cytotoxicity across all cell lines examined and limited selectivity. This behavior is nevertheless consistent with the biological profile typically associated with Ru(II)–arene anticancer compounds, which are often more effective against metastatic or secondary tumors rather than primary tumor models. Among this series, the pyridinium-containing derivative **4e** appears to be the most selective compound, although its overall antiproliferative potency remains modest.

2.6 | Evaluation of the Proapoptotic Activity

The determination of the type of cell death induced by new complexes is crucial not only to assess their efficacy but also to evaluate potential side effects, particularly those related to inflammatory responses. Apoptotic cell death is a tightly regulated process: damaged cells are recognized and removed via phagocytosis, minimizing collateral tissue damage [73]. In contrast, necrosis is an unregulated process, characterized by cell swelling, membrane rupture, and uncontrolled release of intracellular content, which can trigger inflammatory responses [74]. Therefore, the pro-apoptotic potential of the most promising Cu(I) complexes (**2a–d**) was investigated.

Apoptosis was assessed using the Annexin V assay across a range of concentrations, including the IC_{50} for each compound. This method allows discrimination of live cells from those in early or late apoptosis or necrosis, providing both qualitative population distribution and quantitative percentages [75]. Untreated

10990682c, 0, Downloaded from https://chemistry-europe.onlinelibrary.wiley.com/doi/10.1002/ejic.70285 by Universita Di Ferrara, Wiley Online Library on [30/07/2026]. See the Terms and Conditions (https://onlinelibrary.wiley.com/terms-and-conditions) on Wiley Online Library for rules of use; OA articles are governed by the applicable Creative Commons License

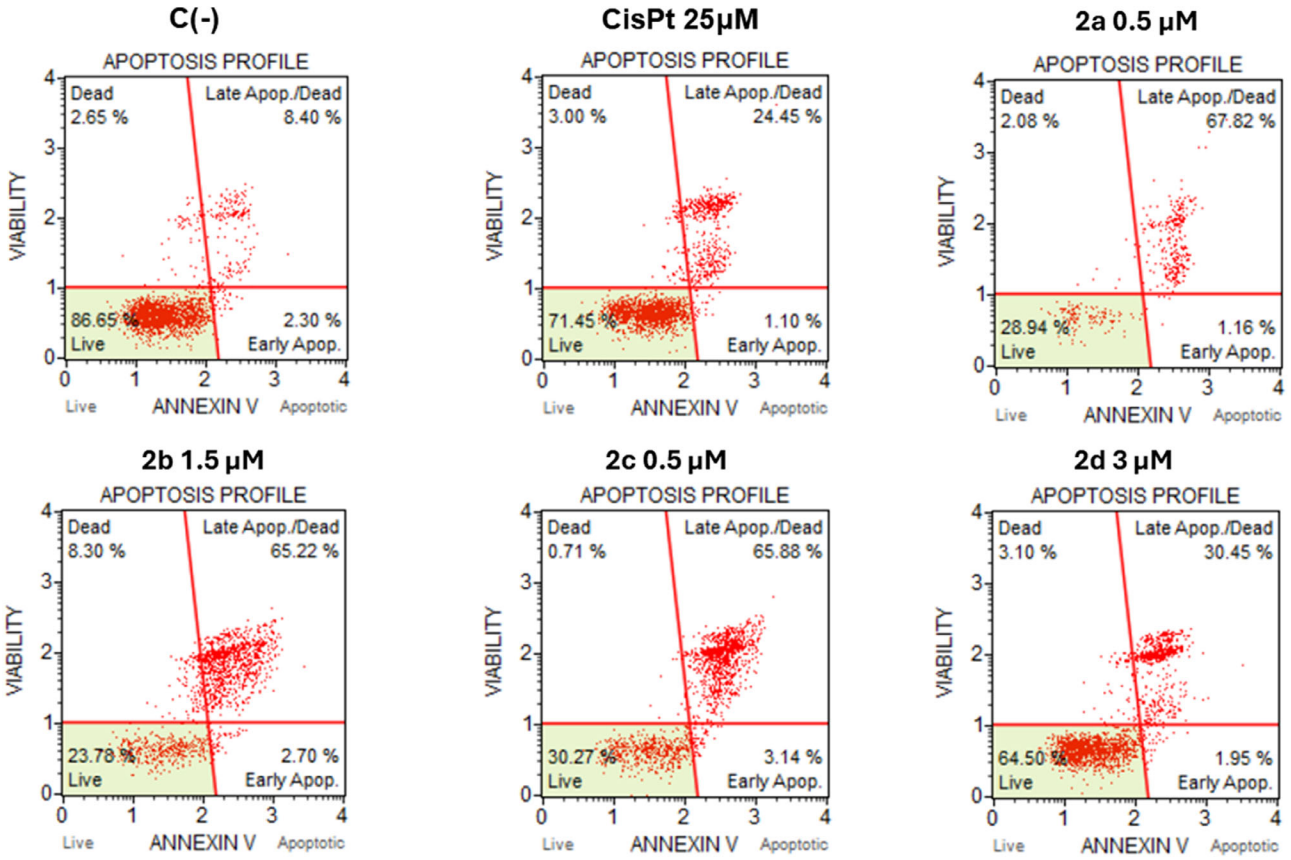

FIGURE 3 | Representative experiments of apoptosis induction on ovarian cancer A2780*cis* cells treated with CisPt and Cu(I)–NHC complexes **2a–d**, in comparison with untreated cells (C-).

controls displayed minimal cell death, confirming the healthy state of the cultures.

In the A2780 ovarian cancer line, the Cu(I) complexes induced apoptosis in a dose-dependent manner, reaching 28%–35% of total apoptosis at the highest concentrations, lower than cisplatin (>65%). However, in the cisplatin-resistant A2780*cis* line, the Cu(I) complexes were highly effective, inducing apoptosis up to 69% at sub-micromolar concentrations (**2c**), whereas cisplatin at 25 µM showed only modest proapoptotic activity (∼25%) (Figure 3). Compound **2d** followed the same trend, albeit with lower apoptotic percentages (∼32%), consistent with IC_{50} data. These results indicate that the copper(I) complexes efficiently overcome cisplatin resistance, inducing predominantly apoptotic cell death.

In MCF-7 breast cancer cells, only the most active complexes (**2a** and **2c**) were tested. Cisplatin showed limited efficacy, inducing 36%–50% apoptosis at the highest concentrations, whereas the Cu(I) complexes reached up to 69% apoptosis at sub-micromolar doses, demonstrating their potential against hormone-sensitive breast tumors.

In nontumorigenic HaCaT keratinocytes, the Cu(I) complexes induced moderate apoptosis (<22%), significantly lower than cisplatin (up to 93%), indicating higher selectivity towards cancer cells.

Overall, these results confirm that the investigated Cu(I) complexes promote effective apoptosis in tumor cells, with pronounced activity in cisplatin-resistant lines and improved selectivity compared to the reference drug. This highlights their potential as anticancer agents capable of overcoming platinum-based resistance mechanisms.

3 | Conclusions

In this work, we have developed an integrated strategy combining innovative synthetic chemistry with biological evaluation to explore how backbone functionalization of NHC ligands modulates the properties of copper(I) and ruthenium(II) metallodrugs. Building on recent advances in the scalable preparation of functionalized imidazolium precursors, notably the multicomponent nucleophilic addition/cyclization approach of Ananikov and coworkers, we demonstrated the operationally simple and efficient synthesis of a series of backbone-modified imidazolium salts bearing chloromethyl, azidomethyl, triazole–steroid, and pyridinium functionalities. The straightforward isolation of these precursors on multigram scale under nonstringent conditions underscores the practical utility of this strategy for accessing complex NHC scaffolds amenable to further diversification.

The backbone functionalization approach enabled the systematic incorporation of biologically relevant motifs while retaining the steric shielding conferred by bulky *N*-aryl substituents. Subsequent conversion of these precursors into Cu(I)–NHC complexes via a weak-base route exemplified an operationally accessible synthetic methodology that avoids the need for strongly

10990682c, 0, Downloaded from https://chemistry-europe.onlinelibrary.wiley.com/doi/10.1002/ejic.70285 by Universita Di Ferrara, Wiley Online Library on [30/07/2026]. See the Terms and Conditions (https://onlinelibrary.wiley.com/terms-and-conditions) on Wiley Online Library for rules of use; OA articles are governed by the applicable Creative Commons License

basic or highly anhydrous conditions, leveraging soluble cuprate intermediates to facilitate carbene generation and coordination. With the exception of the pyridinium-functionalized precursor, which exhibited limited solubility of key intermediates and resulted in decomposition, the synthetic protocol proved general and high-yielding. Structural and spectroscopic characterization confirmed the formation of well-defined linear [Cu(NHC)Cl] complexes.

Complementary efforts in the Ru(II)–arene series employed an analogous weak-base metalation protocol to generate [Ru(η^6-*p*-cymene)(NHC)(CO_3)] species, which could be converted to dichloro derivatives upon treatment with TMSCl. The modularity of this approach allowed direct comparison of carbonato versus dichloro coordination environments and highlighted the influence of ligand architecture on solution behavior. While isolated yields and spectroscopic signatures confirmed successful complexation across most derivatives, certain functional groups, such as azido moieties, underwent unexpected transformations (e.g., conversion to nitrile), likely facilitated by the redox flexibility intrinsic to Ru(II)/Ru(III) systems.

Biological evaluation revealed distinct profiles for the two metallodrug families. The Cu(I)–NHC complexes displayed potent antiproliferative activity across ovarian and breast cancer cell models, including cisplatin-resistant A2780*cis* cells, with IC_{50} values comparable to or better than those of cisplatin. The retention of activity in resistant cells suggests mechanisms of action that diverge from classical platinum-DNA crosslinking, a behavior consistent with emerging evidence that metal–NHC complexes can engage multiple intracellular targets beyond DNA metalation. Importantly, selected copper complexes also exhibited significant induction of apoptosis in tumor cells, while showing comparatively lower apoptotic activity in nontumorigenic keratinocytes, resulting in moderate selectivity that merits further optimization in medicinal chemistry campaigns. Within this series, derivatives such as **2a** and **2c** provided the best overall balance of potency and selectivity.

By contrast, the Ru(II)–NHC complexes demonstrated moderate antiproliferative activity, with IC_{50} values in the 25–50 μM range that are approximately one order of magnitude higher than cisplatin in sensitive cells but comparable to cisplatin in resistant models, suggesting a distinct mechanism with potential benefits in contexts of platinum resistance. This profile is consistent with the broader literature on Ru(II)–arene metallodrugs, which often exhibit multifaceted biological effects including anti-metastatic, anti-angiogenic, or modulatory activities, rather than solely cytotoxic effects driven by direct DNA damage. For these complexes, selectivity toward malignant versus nontumoral cells was limited, though the pyridinium-functionalized species displayed a comparatively more favorable selectivity index, an observation that may inform future ligand design.

Collectively, these findings illustrate how backbone functionalization of NHC ligands can be leveraged to influence both the synthetic accessibility and biological behavior of metallodrugs in a predictable and tunable fashion. The robust activity profiles of the copper(I) complexes, particularly against resistant cancer models, underscore their promise as lead structures for further preclinical development. Future studies will be directed toward elucidating the molecular mechanisms of action underlying their cytotoxic and pro-apoptotic effects, including the potential involvement of regulated cell-death pathways such as cuproptosis, and toward optimizing pharmacokinetic, biodistribution, and safety profiles. Furthermore, the modular design principles established here provide a versatile platform for integrating additional targeting vectors or pharmacophores, paving the way for next-generation anticancer metallodrugs with improved selectivity and therapeutic index.

4 | Experimental

4.1 | Materials and Methods

All solvents and reagents, including metal precursors, were used as purchased (Sigma–Aldrich/Merck).

NMR spectra were recorded by a Bruker 400 MHz spectrometer. Elemental analyses were carried out using an Elemental CHN 'CUBO Micro Vario' analyzer.

4.2 | Growth Inhibition Assays

The human cancer A2780, A2780*cis* and MCF-7 cell lines were maintained in adhesion in RPMI 1640 medium (Euroclone, Milano, Italia), supplemented with 10% fetal bovine serum (FBS; Gibco, Thermo Fisher Scientific, Waltham, MA, USA), 50 units/mL penicillin (Lonza, Verviers, Belgium), and 50 μg/mL streptomycin (Lonza, Verviers, Belgium). To conserve the resistance, 1 μM cisplatin was routinely added to the A2780*cis* cells. The incubation was performed at 37 °C in a 5% CO_2 humidified atmosphere.

The human skin keratinocytes HaCaT were obtained from Istituto Zooprofilattico Sperimentale della Lombardia e dell'Emilia Romagna, Brescia, Italy, and maintained in DMEM (Gibco, Thermo Fisher Scientific, Waltham, MA, USA), supplemented with 10% fetal bovine serum (FBS; Gibco, Thermo Fisher Scientific, Waltham, MA, USA), 50 units mL 1 penicillin (Lonza, Verviers, Belgium), and 50 μg/mL 1 streptomycin (Lonza, Verviers, Belgium). Glutamine (2 mM) was added to the complete medium. The incubation was performed at 37 °C in a 5% CO_2 humidified atmosphere. Cells were detached from the tissue culture or 24-well plates as follows: after a gentle cleanup with 1X PBS, trypsin (100 μL per well) was added. After 5–10 min incubation at 37 °C, FBS (100 μL per well) and proper complete medium (800 μL per well) are added. Cells, harvested and suspended in physiological solution, were counted with a Z2 Coulter Counter (Coulter Electronics, Hialeah, FL, USA). The IC_{50} was calculated after 2–3 days of culture, when untreated cells are in log-growth phase [76].

4.3 | Apoptosis Assays

Annexin V and dead cell assays were carried out after 2–3 days of culture. Cells were treated with different concentrations (IC_{50} and 2X IC_{50} values) of the selected derivatives and were analyzed with a MUSE Cell Analyzer (Millipore, Billerica, MA, USA), according

10990682c, 0, Downloaded from https://chemistry-europe.onlinelibrary.wiley.com/doi/10.1002/ejic.70285 by Universita Di Ferrara, Wiley Online Library on [30/07/2026]. See the Terms and Conditions (https://onlinelibrary.wiley.com/terms-and-conditions) on Wiley Online Library for rules of use; OA articles are governed by the applicable Creative Commons License

to the instructions supplied by the manufacturer. This procedure is based on Annexin V to detect PS (PhosphatidylSerine) on the external membrane of apoptotic cells. Moreover, a dead cell marker, 7-AAD (7-amino-actinomycin D), included in the same kit, was used as an indicator of cell membrane structural integrity. Cells were diluted (1:1) with the one step addition of the Muse Annexin V & Dead Cell reagent. After 20 min of incubation between cell samples and kit at room temperature in the dark, samples were analyzed. Data were acquired and recorded utilizing the Annexin V and Dead Cell Software Module (Millipore, Billerica, MA, USA) [77].

4.4 | Cell Treatment

The derivatives were added to the cell cultures at different concentrations and incubated for 24–48 h (HaCaT), 48–72 h (A2780, MCF-7, A2780*cis*). To prepare both stock solutions (50 mM) and working dilutions, the compounds were dissolved in DMF. Finally, the appropriately diluted compounds were added to wells containing cells in 1 mL of complete medium to achieve the desired final concentrations for cell treatment (the DMF concentration never exceeded 0.2%). In any case, control experiments showed lack of biological effects of the DMF vehicle. Cisplatin (diluted in H_2O) was employed as positive control for all the cell lines, A2780, A2780*cis*, MCF-7, and HaCaT. Untreated cells were placed in every plate as negative control (C-). The vehicle (DMF) was verified as unable to induce antiproliferative/pro apoptotic activity.

4.5 | Synthesis of 2,3-Bis(2,4,6-Trimethylphenyl) butane Diimine

Following the procedure described in the literature [64], 30 mL of 2,4,6-trimethylphenylaniline (28.49 g, 0.21 mol) and 8.83 g of butanedione (0.10 mol) were introduced into a 500 mL round-bottom flask and dissolved in 300 mL of ethanol. Formic acid (2.5 mL) was added dropwise. After stirring at room temperature for 18 h, the diimine product precipitated upon placing the flask in an ice bath. The solid was then isolated by filtration, affording 27.91 g of a yellow powder in 87% yield.

^{1}H NMR (400 MHz, $CDCl_3$, $T = 298$ K, ppm) δ: 2.00 (s, 12H, *o*-CH_3), 2.03 (s, 6H, *p*-CH_3), 2.29 (s, 6H, CH_3), 6.89 (s, 4H, *m*-CH).

4.6 | Synthesis of Imidazolium Salt 1a

Following the procedure described in the literature [65], paraformaldehyde (175 mg, 5.85 mmol, 1.25 equiv.) and 4 M HCl in dioxane (1.81 mL, 7.25 mmol, 1.55 equiv.) were combined and stirred until a clear solution was obtained. This solution was then added dropwise to a suspension of *N*,*N*′-dimesityl-2,3-butanediimine (1.50 g, 4.68 mmol, 1.00 equiv.) in ethyl acetate (20 mL). The resulting mixture was stirred at room temperature for 8 h, during which a white solid gradually formed. The precipitate was collected by filtration and dried under reduced pressure (Yield = 40%).

^{1}H NMR (300 MHz, $CDCl_3$, $T = 298$ K, ppm) δ: 2.06 (s, 6H, CH_3), 2.12 (s, 12H, *o*-CH_3), 2.34 (s, 6H, *p*-CH_3), 7.04 (s, 4H), 10.70 (s, 1H).

4.7 | Synthesis of Imidazolium Salt 1b

According to the procedure described in the literature [55], 15.02 g (0.047 mol) of *N*,*N*′-dimesityl-2,3-butanediimine were dissolved in 100 mL of ethyl acetate in a 250 mL round-bottom flask. Triethyl orthoformate (48 mL) was then added, affording a bright yellow solution. Trimethylsilyl chloride (15 mL, 0.12 mol) was added dropwise, resulting in a color change to red. The reaction mixture was stirred at room temperature for 24 h.

Product **1b** was isolated by filtration and washed with ethyl acetate (2 × 100 mL), yielding 14.92 g of a white powder (79% yield).

^{1}H-NMR (400 MHz, DMSO-d_6, $T = 298$ K, ppm): δ: 2.06 (s, 6H, *o*-CH_3), 2.11 (s, 6H, *o*-CH_3), 2.19 (s, 3H, CH_3), 2.36 (s, 3H, *p*-CH_3), 2.37 (s, 3H, *p*-CH_3), 4.76 (s, 2H, CH_2), 7.23 (s, 4H, *m*-CH), 9.64 (s, 1H, NCHN).

4.8 | Synthesis of Imidazolium Salt 1c

5.03 g (12.5 mmol) of **1b** were dissolved in 65 mL of acetone in a 150 mL round-bottom flask. Sodium azide (2.46 g, 37.8 mmol) was then added, affording a milky suspension. The reaction mixture was stirred at room temperature for 4 h. Product **1c**′ was obtained as a white solid in a 97% yield (5.03 g).

The counterion exchange was carried out as described by dissolving 2.08 g of **1c**′ in 50 mL of methanol in the presence of 3 g of ion-exchange resin (DOWEX-21KCl). The mixture was stirred for 24 h. Product **1c** was isolated by removal of the solvent under reduced pressure, affording 2.03 g (>99% yield).

^{1}H NMR (300 MHz, $CDCl_3$, $T = 298$ K, ppm) δ: 2.13 (s, 6H, *o*-CH_3), 2.16 (s, 6H, *o*-CH_3), 2.19 (s, 3H, CH_3), 2.35 (s, 6H, *p*-CH_3), 4.30 (s, 2H, CH_2), 7.06 (s, 4H, *m*-CH), and 10.90 (s, 1H, NCHN).

4.9 | Synthesis of Imidazolium Salt 1d

Ethisterone (1.00 g, 3.21 mmol) and compound **1c** (1.31 g, 3.20 mmol) were placed in a 250 mL round-bottom flask under an argon atmosphere, followed by the addition of $CHCl_3$ (50 mL), CH_3CN (25 mL), and *tert*-BuOH (25 mL). In two separate vials, $CuSO_4 \cdot 5H_2O$ (0.29 g, 1.2 mmol) and sodium ascorbate (0.67 g, 1.1 mmol) were each dissolved in 12.5 mL of water.

The $CuSO_4$ solution was first added to the reaction flask, resulting in a color change and formation of a brown suspension. Upon addition of the sodium ascorbate solution, the mixture turned milky. The reaction was stirred at 65 °C for 18 h under an argon atmosphere.

The mixture was then subjected to extraction with $CHCl_3/H_2O$. The organic layer was separated, dried over $MgSO_4$, and concentrated under reduced pressure. The resulting solid was redissolved in ethanol and filtered through a PTFE membrane. Removal of the solvent under reduced pressure afforded 2.06 g of compound **1d** as a brownish powder (89% yield).

10990682c, 0, Downloaded from https://chemistry-europe.onlinelibrary.wiley.com/doi/10.1002/ejic.70285 by Universita Di Ferrara, Wiley Online Library on [30/07/2026]. See the Terms and Conditions (https://onlinelibrary.wiley.com/terms-and-conditions) on Wiley Online Library for rules of use; OA articles are governed by the applicable Creative Commons License

^{1}H NMR (400 MHz, $CDCl_3$, $T = 298$ K, ppm) δ: 0.51–1.94 (m, 47H, steroidyl H, CH_3^{im}), 5.64 (m, 3H, CH(CO) + NCH_2), 7.03 (m, 4H, *m*-CH), 7.72 (s, 1H, N–N–N-CH), 9.50 (s, 1H, NCHN).

^{13}C-NMR (101 MHz, $CDCl_3$, $T = 298$ K, ppm) δ: 9.00–53.40 (Steroidyl C alkyl, C CH_3^{im}), 41.97 (C, CH_2), 123.50 C, (Aryl-C), 123.76 (C, CH(CO)), 126.82 (Aryl-C), 128.19 (Aryl-C), 130.16 (Aryl-C), 133.61 (Aryl-C), 134.59 (Aryl-C), 134.62 (Aryl-C), 135.07 (C, NCHN), 136.22 (Aryl-C), 142.01 (Aryl-C), 142.23 (Aryl-C), 154.12 (Aryl-C), 171.43, 199.52 (C=O).

4.10 | Synthesis of Imidazolium Salt 1e

According to the literature procedure [55], 2.05 g (5.0 mmol) of **1b** were combined with pyridine (35 mL, 80 equiv.) in a 100 mL round-bottom flask. The reaction mixture was stirred at 85 °C overnight.

Diethyl ether (100 mL) was then added, and the resulting solid was collected by filtration. The solid was washed with diethyl ether (2 × 50 mL) and dried under reduced pressure to afford 2.12 g of product **1e** as a brownish solid (86% yield).

^{1}H NMR (400 MHz, DMSO-d_6, $T = 298$ K, ppm) δ: 1.70 (s, 6H, *o*-CH_3), 2.06 (s, 6H, *o*-CH_3), 2.32 (s, 6H, *p*-CH_3), 2.34 (s, 3H, CH_3), 5.90 (s, 2H, CH_2), 7.05 (s, 2H, *m*-CH), 7.21 (s, 2H, *m*-CH), 7.97–8 (m, 2H, H-py$^+$), 8.55–8.62 (m, 3H, H-py$^+$), 9.62 (s, 1H, NCHN).

4.11 | Synthesis of Complex 2a

Compound **1a** (100 mg, 0.27 mmol), CuCl (26.8 mg, 0.27 mmol), and K_2CO_3 (112.3 mg, 0.81 mmol) were added in a vial, followed by the addition of technical-grade acetone (2 mL). The reaction mixture was stirred at 60 °C for 24 h.

Upon completion, the solvent was removed under reduced pressure. The resulting crude solid was redissolved in CH_2Cl_2 (5 mL), and the solution was passed through a short pad of silica gel using CH_2Cl_2 as the eluent. Removal of the solvent under reduced pressure afforded complex **2a** (101.6 mg) as a white solid (87% yield).

^{1}H NMR (300 MHz, $CDCl_3$, $T = 298$ K, ppm) δ: 1.90 (s, 6H, CH_3), 2.03 (s, 12H, *o*-CH3), 2.34 (s, 6H, *p*-CH_3), 6.99 (s, 4H, *m*-CH).

^{13}C NMR (101 MHz, $CDCl_3$, $T = 298$ K, ppm) δ: 9.19 (C, CH_3^{im}), 17.89 (C, *o*-CH_3), 21.27 (C, *p*-CH_3), 125.54 (C, Aryl-C), 129.60 (C, Aryl-C), 133.81 (C, Aryl-C), 135.05 (C, Aryl-C), 139.33 (C, Aryl-C), 175.47 (C, Carbene).

Elemental analysis calcd (%) for $C_{23}H_{28}ClCuN_2$: C, 64.02; H, 6.54; N, 6.49; found: C, 64.37; H, 6.41; N, 6.34.

4.12 | Synthesis of Complex 2b

Compound **1b** (100.5 mg, 0.25 mmol), CuCl (24.8 mg, 0.25 mmol), and K_2CO_3 (102.6 mg, 0.74 mmol) were added in a vial, followed by the addition of technical-grade acetone (2 mL). The reaction mixture was stirred at 60 °C for 24 h.

Upon completion, the solvent was removed under reduced pressure. The resulting crude solid was redissolved in CH_2Cl_2 (5 mL), and the solution was passed through a short pad of silica gel using CH_2Cl_2 as the eluent. Removal of the solvent under reduced pressure afforded complex **2b** (97.4 mg) as a white solid (83% yield).

^{1}H NMR (400 MHz, $CDCl_3$, $T = 298$ K, ppm) δ: 2.01 (s, 3H, CH_3), 2.03 (s, 6H, *o*-CH_3), 2.07 (s, 6H, *o*-CH_3), 2.35 (s, 6H, *p*-CH_3), 4.27 (s, 2H, CH_2), 7.01 (s, 4H, *m*-CH)

^{13}C NMR (101 MHz, Chloroform-*d* $T = 298$ K, ppm) δ: 9.22 (C. CH3^{im}), 17.76 (*o*-CH_3), 18.07 (*o*-CH_3), 21.25 (*p*-CH_3), 33.57 (*p*-CH_3), 129.82 (C, Aryl-C), 134.84 (C, Aryl-C), 135.30, 139.98 (C, Aryl-C), 178.08 (C, carbene).

Elemental analysis calcd (%) for $C_{23}H_{27}Cl_2CuN_2$: C, 59.29; H, 5.84; N, 6.01; found: C, 59.50; H, 5.69; N, 5.93.

4.13 | Synthesis of Complex 2c

Compound **1c** (150 mg, 0.37 mmol), CuCl (36.2 mg, 0.37 mmol), and K_2CO_3 (151.7 mg, 1.10 mmol) were added in a vial, followed by the addition of technical-grade acetone (2 mL). The reaction mixture was stirred at 60 °C for 24 h.

Upon completion, the solvent was removed under reduced pressure. The resulting crude solid was redissolved in CH_2Cl_2 (5 mL), and the solution was passed through a short pad of silica gel using CH_2Cl_2 as the eluent. Removal of the solvent under reduced pressure afforded complex **2c** (103.2 mg) as a brownish solid (60% yield).

^{1}H NMR (400 MHz, $CDCl_3$, $T = 298$ K, ppm) δ: 2.04 (s, 3H, CH_3), 2.07 (s, 6H, *o*-CH_3), 2.09 (s, 6H, *o*-CH_3), 2.37 (s, 6H, *p*-CH_3), 4.07 (s, 2H, CH_2), 7.04 (s, 4H, *m*-CH).

^{13}C NMR (101 MHz, $CDCl_3$, $T = 298$ K, ppm) δ: 9.28 (C, CH_3^{im}), 17.77 (C, *o*-CH_3), 21.19 (C, *p*-CH_3), 21.20 (*p*-CH_3), 43.20 (*p*-CH_3), 124.01(C, Aryl-C), 129.71(C, Aryl-C), 129.76(C, Aryl-C), 132.52 (C, Aryl-C), 132.97 (C, Aryl-C), 134.83 (C, Aryl-C), 135.12 (C, Aryl-C), 139.78 (C, Aryl-C), 139.92 (C, Aryl-C), 178.16 (C, carbene).

Elemental analysis calcd (%) for $C_{23}H_{27}ClCuN_5$: C, 58.47; H, 5.76; N, 14.82; found: C, 58.20; H, 5.89; N, 14.61.

4.14 | Synthesis of Complex 2d

Compound **1d** (150 mg, 0.21 mmol), CuCl (20.5 mg, 0.21 mmol), and K_2CO_3 (86.0 mg, 0.62 mmol) were added in a vial, followed by the addition of technical-grade acetone (2 mL). The reaction mixture was stirred at 60 °C for 24 h.

Upon completion, the solvent was removed under reduced pressure. The resulting crude solid was redissolved in CH_2Cl_2 (5 mL), and the solution was passed through a short pad of silica gel

10990682c, 0, Downloaded from https://chemistry-europe.onlinelibrary.wiley.com/doi/10.1002/ejic.70285 by Universita Di Ferrara, Wiley Online Library on [30/07/2026]. See the Terms and Conditions (https://onlinelibrary.wiley.com/terms-and-conditions) on Wiley Online Library for rules of use; OA articles are governed by the applicable Creative Commons License

using CH_2Cl_2 as the eluent. Removal of the solvent under reduced pressure afforded complex **2d** (136.7 mg) as a brownish solid (84% yield).

^{1}H NMR (400 MHz, $CDCl_3$, $T = 298$ K, ppm) δ: 0.36–2.42, (47H, Steroidyl H, CH_3^{im}), 5.06–5.17 (m, 2H. NCH_2), 5.69 (s. 1H, CH(CO)), 6.63 (s, 1H, N–N–N-CH), 6.90–7.00 (m, 4H, *m*-CH).

^{13}C NMR (101 MHz, $CDCl_3$, $T = 298$ K, ppm) δ: 1.14–53.51 (Steroidyl C alkyl, C CH_3^{im}), 42.66 (C, NCH_2), 121.72 (C. NNCH), 124.02 (C, CH(CO)), 129.84 (C, Aryl-C), 129.86 (C, Aryl-C), 129.95 (C, Aryl-C), 129.99 (C, Aryl-C), 132.46 (C, Aryl-C), 132.97 (C, Aryl-C), 134.81 (C, Aryl-C), 134.86(C, Aryl-C), 135.24 (C, Aryl-C), 135.46 (C, Aryl-C), 140.00 (C, Aryl-C), 140.36 (C, Aryl-C), 178.18 (C, Carbene), 199.40 (C=O).

Elemental analysis calcd (%) for $C_{44}H_{55}ClCuN_5O_2$: C, 67.33; H, 7.06; N, 8.92; found: C, 67.52; H, 6.94; N, 8.77.

4.15 | Synthesis of Cuprate Complex $[CuCl_2][IMes^{CH3,CH2Cl}.H]$

Compound **1b** (20.8 mg, 0.05 mmol) and CuCl (5.3 mg, 0.05 mmol) were added in a vial, followed by the addition of technical-grade acetone (2 mL). The reaction mixture was stirred at 60 °C for 30 min.

Upon completion, removal of the solvent under reduced pressure afforded the target cuprate complex in a quantitative yield.

^{1}H NMR (400 MHz, $CDCl_3$, $T = 298$ K, ppm) δ: 2.11 (s, 6H, *o*-CH_3), 2.15 (s, 6H, *o*-CH_3), 2.26 (s, 3H, CH_3), 2.40 (s, 6H, *p*-CH_3), 4.47 (s, 2H, CH_2), 7.12 (s, 4H, *m*-CH), 9.11 (s, 1H, NCHN).

4.16 | Synthesis of Cuprate Complex $[CuCl_2][IMes^{CH3,CH2Py}.H]$

Compound **1e** (70.1 mg, 0.15 mmol) and CuCl (14.6 mg, 0.15 mmol) were added in a vial, followed by the addition of technical-grade acetone (2 mL). The reaction mixture was stirred at 60 °C for 30 min.

Upon completion, removal of the solvent under reduced pressure afforded the target cuprate complex in a quantitative yield.

^{1}H NMR (400 MHz, $CDCl_3$, $T = 298$ K, ppm) δ: 1.76 (s, 3H, CH_3), 2.04 (m, 6H, *o*-CH_3), 2.20 (s, 6H, *o*-CH_3), 2.38 (m, 6H, *p*-CH_3), 2.70 (s, 2H, CH_2), 7.05 (m, 6H, *m*-CH + CH_2), 7.99 (d, $J = 40.7$ Hz, 2H, H-py$^+$), 8.54 (s, 2H, H-py$^+$), 9.01 (s, 1H, H-py$^+$), 9.84 (s, 1H, NCHN).

4.17 | Synthesis of Complex 3a

Compound **1a** (150 mg, 0.41 mmol), $[RuCl_2(p\text{-cymene})]_2$ (124.5 mg, 0.20 mmol), and K_2CO_3 (280.9 mg, 2.03 mmol) were added in a vial, followed by the addition of technical-grade acetone (2 mL). The reaction mixture was stirred at 60 °C for 18 h.

Upon completion, the solvent was removed under reduced pressure. The resulting crude solid was redissolved in CH_2Cl_2 (5 mL) and then filtered on a PTFE membrane. Removal of the solvent under reduced pressure afforded complex **3a** (181.5 mg) as a brown solid (71% yield).

^{1}H NMR (400 MHz, $CDCl_3$, $T = 298$ K, ppm) δ: 0.80 (d, $J = 6.9$ Hz, 6H, cymene-CH_3), 1.29 (s, 3H, cymene-CH_3), 1.65 (hep, 6.9 Hz, 1H, cymene-CH), 2.04 (s, 6H, CH_3^{im}), 2.12 (s, 12H, *o*-CH_3), 2.34 (s, 6H, *p*-CH_3), 4.76 (d, $J = 6.0$ Hz, 2H, cymene-CH), 5.11 (d, $J = 5.9$ Hz, 2H, cymene-CH), 7.02 (m Hz, 4H, *m*-CH^{im}).

^{13}C NMR (101 MHz, $CDCl_3$, $T = 298$ K, ppm) δ: 8.60 (C, $CH3^{im}$), 9.37 (C, Alkyl-C), 16.70 (C, Alkyl-C), 17.65 (C, Alkyl-C), 18.74 (C, Alkyl-C), 21.03 (C, Alkyl-C), 21.20 (C, Alkyl-C), 23.37 (C, Alkyl-C), 31.74 (C, Alkyl-C), 83.54 (C, cymene), 84.80 (C, cymene), 94.57 (C, cymene), 99.25 (C, cymene), 127.31 (C, Aryl-C), 128.86 (C, Aryl-C), 128.91 (C, Aryl-C), 129.98 (C, Aryl-C), 134.66 (C, Aryl-C), 134.81 (C, Aryl-C), 136.91 (C, Aryl-C), 138.60 (C, Aryl-C), 141.27 (C, Aryl-C), 166.35 (C, carbonate), 176.35 (C, carbene).

Elemental analysis calcd (%) for $C_{34}H_{42}N_2O_3Ru$: C, 65.05; H, 6.74; N, 4.46; found: C, 65.36; H, 6.58; N, 4.38.

4.18 | Synthesis of Complex 3b

Compound **1b** (150 mg, 0.41 mmol), $[RuCl_2(p\text{-cymene})]_2$ (124.5 mg, 0.20 mmol), and K_2CO_3 (280.9 mg, 2.03 mmol) were added in a vial, followed by the addition of technical-grade acetone (2 mL). The reaction mixture was stirred at 60 °C for 18 h.

Upon completion, the solvent was removed under reduced pressure. The resulting crude solid was redissolved in CH_2Cl_2 (5 mL) and then filtered on a PTFE membrane. Removal of the solvent under reduced pressure afforded complex **3b** (181.5 mg) as a brown solid (71% yield).

^{1}H NMR (400 MHz, $CDCl_3$, $T = 298$ K, ppm) δ: 0.77 (d, $J = 6.8$ Hz, 6H, cymene-CH_3), 1.25 (s, 3H, cymene-CH_3), 1.60 (hep, $J = 6.6$ Hz, 1H, cymene-CH), 1.86 (s, 3H, CH_3^{im}), 2.09 (6H, *o*-CH_3), 2.11 (6H, *o*-CH_3), 2.30 (3H, *p*-CH_3), 2.32 (3H, *p*-CH_3) 4.12 (s, 2H, CH_2^{im}), 4.72 (d, $J = 5.9$ Hz, 2H, cymene-CH), 5.07 (d, $J = 5.9$ Hz, 2H, cymene-CH), 6.94 (d, $J = 11.7$ Hz, 4H, *m*-CH^{im}).

^{13}C NMR (101 MHz, $CDCl_3$, $T = 298$ K, ppm) δ: 9.35 (C, CH_3^{im}), 16.69 (C, Alkyl-C), 18.76 (C, Alkyl-C), 18.83 (C, Alkyl-C), 19.04 (C, Alkyl-C), 21.05 (C, Alkyl-C), 21.06 (C, Alkyl-C), 21.09 (C, Alkyl-C), 23.40 (C, Alkyl-C), 31.84,(C, Alkyl-C) 53.76 (C, CH_2), 83.49 (C, cymene), 84.90 (C, cymene), 94.74 (C, cymene), 99.28 (C, cymene), 128.93 (C, Aryl-C), 129.21 (C, Aryl-C), 130.29 (C, Aryl-C), 130.90 (C, Aryl-C), 134.32 (C, Aryl-C), 134.63 (C, Aryl-C), 138.68 (C, Aryl-C), 139.64 (C, Aryl-C), 166.35 (C, carbonate), 178.35 (C, carbene).

10990682c, 0, Downloaded from https://chemistry-europe.onlinelibrary.wiley.com/doi/10.1002/ejic.70285 by Universita Di Ferrara, Wiley Online Library on [30/07/2026]. See the Terms and Conditions (https://onlinelibrary.wiley.com/terms-and-conditions) on Wiley Online Library for rules of use; OA articles are governed by the applicable Creative Commons License

Elemental analysis calcd (%) for $C_{34}H_{41}ClN_2O_3Ru$: C, 61.67; H, 6.24; N, 4.23; found: C, 61.90; H, 6.12; N, 4.09.

4.19 | Synthesis of Complex 3c*

Compound **1c** (121.0 mg, 0.30 mmol), $[RuCl_2(p\text{-cymene})]_2$ (89.5 mg, 0.15 mmol), and K_2CO_3 (202.4 mg, 1.46 mmol) were added in a vial, followed by the addition of technical-grade acetone (2 mL). The reaction mixture was stirred at 60 °C for 18 h.

Upon completion, the solvent was removed under reduced pressure. The resulting crude solid was redissolved in CH_2Cl_2 (5 mL) and filtered through a PTFE membrane. Removal of the solvent under reduced pressure afforded complex **3c*** (157.4 mg) as a brown solid (84% yield).

Unfortunately, only a small fraction of this compound could be isolated in sufficiently pure form after multiple recrystallizations, yielding enough material for crystal growth suitable for X-ray diffraction (XRD) analysis.

^{1}H NMR (400 MHz, $CDCl_3$, $T = 298$ K, ppm) δ: 0.81 (d, $J = 6.9$ Hz, 6H, CH_3 del cymene), 1.32 (s, 3H, cymene-CH_3), 1.68 (hep, $J = 6.9$ Hz, 1H, cymene-CH), 2.03 (s, 3H, CH_3^{im}), 2.15 (6H, *o*-CH_3), 2.22 (6H, *o*-CH_3), 2.36 (6H, *p*-CH_3), 4.77 (d, $J =$ 5.9 Hz, 2H, cymene-CH), 5.14 (d, $J = 5.9$ Hz, 2H, cymene-CH), 7.02–7.11 (m, $J = 11.7$ Hz, 4H, *m*-CH^{im}).

4.20 | Synthesis of Complex 3d

Compound **1d** (100.9 mg, 0.14 mmol), $[RuCl_2(p\text{-cymene})]_2$ (42.4 mg, 0.07 mmol), and K_2CO_3 (95.7 mg, 0.70 mmol) were added in a vial, followed by the addition of technical-grade acetone (2 mL). The reaction mixture was stirred at 60 °C for 18 h.

Upon completion, the solvent was removed under reduced pressure. The resulting crude solid was redissolved in CH_2Cl_2 (5 mL) and filtered through a PTFE membrane. Removal of the solvent under reduced pressure afforded complex **3d** (125 mg) as a brown solid (92% yield).

^{1}H NMR (400 MHz, $CDCl_3$, $T = 298$ K, ppm) δ: 0.07–2.68 (58H, steroidyl H, CH_3^{im} + CH cymene), 4.70–4.76 (3H, CH(CO) + NCH_2), 5.10 (2H, CH cymene), 5.71 (2H, CH cymene), 6.41 (1H, N–N–N-CH), 6.92- 7.10 (4H, *m*-CH).

^{13}C NMR (101 MHz, $CDCl_3$, $T = 298$ K, ppm) δ: 9.58–53.82 (Steroidyl C alkyl, C CH_3^{im}), 83.39 (C, NCH_2), 83.83 (C, NCH_2), 85.02 (C, NNCH), 85.28 (C, NNCH), 95.17 (C, CH(CO), 99.60 (C, CH(CO), 121.80 (C, Aryl-C), 123.88 (C, Aryl-C), 124.98 (C, Aryl-C), 126.27 (C, Aryl-C), 128.97 (C, Aryl-C), 129.11 (C, Aryl-C), 129.37 (C, Aryl-C), 133.07 (C, Aryl-C), 133.60 (C, Aryl-C), 134.33 (C, Aryl-C), 137.04 (C, Aryl-C), 139.25 (C, Aryl-C), 139.35 (C, Aryl-C), 153.33 (C, Aryl-C), 166.25 (C=O, Carbonate), 170.99 (C, Carbene), 181.80 (C, Carbene), 199.41 (C=O), 210.85 (C=O).

Elemental analysis calcd (%) for $C_{55}H_{69}N_5O_5Ru$: C, 67.32; H, 7.09; N, 7.14; found: C, 67.07; H, 7.20; N, 7.23.

4.21 | Synthesis of $[Ru(p\text{-Cymene})Cl_3][IMes^{CH3,CH2Cl}.H]$

Compound **1b** (20.0 mg, 0.05 mmol) and $[RuCl_2(p\text{-cymene})]_2$ (15.3 mg, 0.025 mmol) were added in a vial, followed by the addition of technical-grade acetone (2 mL). The reaction mixture was stirred at 60 °C for 30 min.

Upon completion, removal of the solvent under reduced pressure afforded the target ruthenate complex in a quantitative yield.

^{1}H NMR (400 MHz, CD_3CN, $T = 298$ K, ppm) δ: 1.31 (d, $J = 7.0$ Hz, 6H, CH_3 cymene), 2.11 (s, 3H, CH_3), 2.16 (s, 6H, *o*-CH_3), 2.18 (s, 6H, *o*-CH_3), 2.33 (s, 3H, CH_3), 2.41 (m, 6H, *p*-CH_3), 2.92 (sept, $J = 6.9$ Hz, 1H, CH cymene), 4.56 (s, 2H, CH_2), 5.28 (s, 2H, CH cymene), 5.53 (s, 2H, CH cymene), 7.22 (m, 4H, *m*-CH^{im}), 9.50 (s, 1H, s, 1H, NCHN).

4.22 | Synthesis of $[Ru(p\text{-Cymene})Cl_3][IMes^{CH3,CH2Py}.H]$

Compound **1e** (70.0 mg, 0.15 mmol) and $[RuCl_2(p\text{-cymene})]_2$ (44.4 mg, 0.075 mmol) were added in a vial, followed by the addition of technical-grade acetone (2 mL). The reaction mixture was stirred at 60 °C for 30 min.

Upon completion, removal of the solvent under reduced pressure afforded the target ruthenate complex in a quantitative yield.

^{1}H NMR (400 MHz, CD_3CN, $T = 298$ K, ppm) δ: 1.31 (d, $J = 6.9$ Hz, 6H, cymene-CH_3), 1.82 (s, 6H, *p*-CH_3), 2.16 (s, 6H, o-CH_3), 2.19 (s, 3H, CH_3), 2.42 (s, 6H, *o*-CH_3), 2.49 (s, 3H, CH_3), 2.93 (h, $J = 6.9$, 6.4 Hz, 1H, CH cymene) 5.30 (s, 2H, CH cymene), 5.55 (2H, CH cymene), 6.06 (s, 2H, CH_2^{im}), 7.08–7.23 (m, 4H, *m*-CH^{im}), 7.90 (m, 2H, H-py^+), 8.51(m, 3H, H-py^+), 9.47(s, 1H, NCHN).

4.23 | Synthesis of Complex 4a

Compound **3a** (60.0 mg, 0.18 mmol) was dissolved in THF (2 mL) in a vial, followed by the addition of TMSCl (99.4 mg, 0.91 mmol). The reaction mixture was stirred at room temperature for 5 min.

Upon completion, the solvent was removed under reduced pressure. The resulting solid was redissolved in diethyl ether and precipitated by addition of pentane. The product was isolated to afford compound **4a** (59.3 mg) in 98% yield.

^{1}H NMR (400 MHz, $CDCl_3$, $T = 298$ K, ppm) δ: 1.07 (d, $J = 6.9$ Hz, 6H, cymene-CH_3), 1.70 (s, 6H, CH_3^{im}), 1.76 (s, 3H, cymene-CH_3), 1.84 (m, 1H, cymene-CH), 2.15 (s, 12H, *o*-CH_3), 2.34 (s, 6H, *p*-CH_3), 4.60 (d, $J = 5.9$ Hz, 2H, cymene-CH_2), 5.00 (d, $J = 5.9$ Hz, 2H, cymene-CH_2), 6.94 (s, 4H, *m*-CH).

^{13}C NMR (101 MHz, $CDCl_3$, $T = 298$ K, ppm) δ: 9.74 (C, CH_3^{im}), 18.06 (C, Alkyl-C), 19.20 (C, Alkyl-C), 21.18 (C, Alkyl-C), 22.67 (C, Alkyl-C), 24.11 (C, Alkyl-C), 30.32 (C, Alkyl-C), 33.68 (C, Alkyl-C), 85.72 (C, cymene), 86.69 (C, cymene), 95.56 (C, cymene), 102.30 (C, cymene), 126.28 (C, cymene), 127.56

10990682c, 0, Downloaded from https://chemistry-europe.onlinelibrary.wiley.com/doi/10.1002/ejic.70285 by Universita Di Ferrara, Wiley Online Library on [30/07/2026]. See the Terms and Conditions (https://onlinelibrary.wiley.com/terms-and-conditions) on Wiley Online Library for rules of use; OA articles are governed by the applicable Creative Commons License

(C, cymene), 128.79 (C, Aryl-C), 128.98 (C, Aryl-C), 129.12 (C, Aryl-C), 130.47 (C, Aryl-C), 135.15 (C, Aryl-C), 136.61 (C, Aryl-C), 136.75 (C, Aryl-C), 138.43 (C, Aryl-C), 168.11 (C, Carbene).

Elemental analysis calcd (%) for $C_{33}H_{42}Cl_2N_2Ru$: C, 62.06; H, 6.63; N, 4.39; found: C, 62.39; H, 6.51; N, 4.27.

4.24 | Synthesis of Complex 4b

Compound **3b** (59.9 mg, 0.09 mmol) was dissolved in THF (2 mL) in a vial, followed by the addition of TMSCl (49.6 mg, 0.46 mmol). The reaction mixture was stirred at room temperature for 5 min.

Upon completion, the solvent was removed under reduced pressure. The resulting solid was redissolved in diethyl ether and precipitated by addition of pentane. The product was isolated to afford compound **4b** (60.3 mg) in 98% yield.

^{1}H NMR (400 MHz, $CDCl_3$, $T = 298$ K, ppm) δ: 1.08 (d, $J = 6.9$ Hz, 6H, cymene-CH_3), 1.21 (m, 4H, CH_3 + cymene-CH), 1.81 (s, 3H, CH_3), 2.19 (s 12H, *o*-CH_3), 2.35 (s, 6H, *p*-CH_3), 4.14 (s, 2H, CH_2), 4.57 (d, $J = 5.9$ Hz, 2H, cymene-CH), 5.00 (d, $J = 5.9$ Hz, 2H, cymene-CH), 6.96 (m, 4H, *m*-CH^{im}).

^{13}C NMR (101 MHz, $CDCl_3$, $T = 298$ K, ppm) δ: 9.83 (C, $CH_3{}^{im}$), 15.28 (C, Alkyl-C), 18.13 (C, Alkyl-C), 19.24 (C, Alkyl-C), 19.42 (C, Alkyl-C), 20.96 (C, Alkyl-C), 21.18 (C, Alkyl-C), 21.22(C, Alkyl-C), 22.64 (C, Alkyl-C), 24.10 (C, Alkyl-C), 30.35 (C, Alkyl-C), 33.68 (C, Alkyl-C), 53.92 (C, CH_2), 85.94 (C, cymene), 86.67 (C, cymene), 102.51 (C, cymene), 126.28 (C, cymene), 128.91 (C, cymene), 128.98 (C, Aryl-C), 129.07 (C, Aryl-C), 130.75 (C, Aryl-C), 136.63 (C, Aryl-C), 136.80 (C, Aryl-C), 138.80 (C, Aryl-C), 138.96 (C, Aryl-C), 170.62 (C, Carbene).

Elemental analysis calcd (%) for $C_{33}H_{41}Cl_3N_2Ru$: C, 58.88; H, 6.14; N, 4.16; found: C, 59.03; H, 6.04; N, 4.22.

4.25 | Synthesis of Complex 4d

Compound **3d** (40.8 mg, 0.08 mmol) was dissolved in THF (2 mL) in a vial, followed by the addition of TMSCl (22.1 mg, 0.20 mmol). The reaction mixture was stirred at room temperature for 5 min.

Upon completion, the solvent was removed under reduced pressure. The resulting solid was redissolved in diethyl ether and precipitated by addition of pentane. The product was isolated to afford compound **4d** (40.7 mg) in 98% yield.

^{1}H NMR (400 MHz, $CDCl_3$, $T = 298$ K, ppm) δ: 0.86–2.86 (58H, Steroidyl H, + $CH_3{}^{im}$ + H^{cym}), 4.85–4.95 (3H, CH(CO) + NCH_2), 5.33 (2H, CH cymene), 5.46 (2H, CH cymene), 5.70 (1H, N–N–N-CH), 6.96- 7.10 (4H, *m*-CH).

^{13}C NMR (101 MHz, $CDCl_3$, $T = 298$ K, ppm) δ 14.21–53.85 (Steroidyl C alkil, C $CH_3{}^{im}$, C cym, 80.57 (C, NCH_2), 81.33 (C, CH(CO), 129.31 (C, Aryl-C), 129.54 (C, Aryl-C), 145.92 (C, Aryl-C), 177.90 (C, Carbene), 199.65 (C=O).

Elemental analysis calcd (%) for $C_{54}H_{69}Cl_2N_5O_2Ru$: C, 65.37; H, 7.01; N, 7.06; found: C, 65.01; H, 7.13; N, 7.27.

4.26 | Synthesis of Complex 4e

To a 100 mL round-bottom flask under an inert argon atmosphere, 150.5 mg (0.312 mmol) of compound **1e** and 43.7 mg (0.189 mmol) of Ag_2O were added. Anhydrous DCM (20 mL) was added to dissolve the imidazolium salt. The resulting solution was stirred at room temperature under an inert atmosphere for 16 h. Afterward, the brown solution was filtered through a PTFE microfilter and washed with an additional 20 mL of DCM. The solvent was then evaporated under reduced pressure. After drying, 180.4 mg of the red silver complex **5** was obtained in a 98% yield.

Subsequently, a Schlenk flask was charged with 0.0711 g (0.12 mmol) of the silver complex **5** and 0.0371 g (0.06 mmol) of $[RuCl_2(p\text{-cymene})]_2$ in 15 mL of anhydrous DCM. The reaction mixture was stirred for 30 min at room temperature. The crude mixture was filtered through PTFE, and the product was isolated via recrystallization from diethyl ether, affording 0.0846 g of **4e** (98% yield).

^{1}H NMR (400 MHz, $CDCl_3$, $T = 298$ K, ppm) δ: 1.27 (d, 6H, CH_3 del cymene) 1.65 (s, 3H, CH_3), 1.66 (s, 3H, CH_3), 1.96 (s, 6H, *o*-CH_3), 2.18 (s, 6H, *o*-CH_3), 2.35 (s, 6H, *p*-CH_3), 3.00 (h, 1H, CH cymene) 5.14 (d, 2H, CH cymene), 5.36 (d, 2H, CH cymene), 5.84 (s, 2H, CH_2), 6.90–7.00 (m, 4H, *m*-CH^{im}), 7.68 (m, 2H, H-py^+), 8.00 (m, 2H, H-py^+), 8.19(s, 1H, H-py^+).

^{13}C NMR (101 MHz, $CDCl_3$, $T = 298$ K, ppm) δ: 15.28 (C, Alkyl-C), 17.59 (C, Alkyl-C), 17.80 (C, Alkyl-C), 18.24 (C, Alkyl-C), 18.75 (C, Alkyl-C), 21.17 (C, Alkyl-C), 21.20 (C, Alkyl-C), 21.25 (C, Alkyl-C), 22.16 (C, Alkyl-C), 22.25 (C, Alkyl-C), 22.28 (C, Alkyl-C), 24.10 (C, Alkyl-C), 30.73 (C, Alkyl-C), 65.86 (C, CH_2), 79.60 (C, cymene), 80.55 (C, cymene), 81.31 (C, cymene), 81.59 (C, cymene), 82.20 (C, cymene), 82.88 (C, cymene), 96.37 (C, Aryl-C), 100.91 (C, Aryl-C), 124.56 (C, Aryl-C), 126.28 (C, Aryl-C), 127.66 (C, Aryl-C), 128.20 (C, Aryl-C py^+), 128.98 (C, Aryl-C), 129.93 (C, Aryl-C), 130.11 (C, Aryl-C), 130.16 (C, Aryl-C), 130.26 (C, Aryl-C), 132.35 (C, Aryl-C), 132.89 (C, Aryl-C), 134.49 (C, Aryl-C), 134.87 (C, Aryl-C), 135.14 (C, Aryl-C, py^+), 135.19 (C, Aryl-C, py^+), 137.62 (C, Aryl-C), 140.23 (C, Aryl-C), 141.07 (C, Aryl-C), 141.96 (C, Aryl-C), 142.53 (C, Aryl-C), 144.60 (C, Aryl-C, py^+), 145.10 (C, Aryl-C, py^+), 154.89 (C, Aryl-C, py^+).

Elemental analysis calcd (%) for $C_{38}H_{46}Cl_3N_3Ru$: C, 60.68; H, 6.16; N, 5.59; found: C, 60.40; H, 6.29; N, 5.71.

4.27 | Crystal Structure Determination

$[CuCl_2][IMes^{CH3,CH2Cl}{\cdot}H]$ and **3c*** diffraction data were collected at XRD2 beamline of Elettra Synchrotron, Trieste (Italy) [78], using a monochromatic wavelength of 0.620 Å at 100 K. The data sets were integrated, scaled, and corrected for Lorentz, absorption, and polarization effects using XDS package [79]. SADABS program [80] has been used to scale and apply

10990682c, 0, Downloaded from https://chemistry-europe.onlinelibrary.wiley.com/doi/10.1002/ejic.70285 by Universita Di Ferrara, Wiley Online Library on [30/07/2026]. See the Terms and Conditions (https://onlinelibrary.wiley.com/terms-and-conditions) on Wiley Online Library for rules of use; OA articles are governed by the applicable Creative Commons License

semi-empirical absorption corrections on **3c*** datasets, exploiting multiple measures of symmetry-related reflections. The structures were solved by direct methods using SHELXT program [81] and refined using full−matrix least−squares implemented in SHELXL−2019/3 [82]. Thermal motions for all non−hydrogen atoms have been treated anisotropically. Hydrogens have been included on calculated positions, riding on their carrier atoms. The Coot program was used for structure building [83]. The crystal data are given in Supporting Information. Pictures were prepared using Ortep3 [84] and Pymol software [85].

Crystallographic data have been deposited at the Cambridge Crystallographic Data Centre and allocated the deposition numbers CCDC 2518344 for **[$CuCl_2$][$IMes^{CH3,CH2Cl}$·H]** and 2518345 for **3c*** at 100 K. These data can be obtained free of charge via https://www.ccdc.cam.ac.uk/structures.

Acknowledgments

T.S. gratefully acknowledges the financial support provided by the Department of Chemical Sciences (PDiSC 2024 project "EasyBackTherapy"). I.L. was financially supported by FAR 2023 (University of Ferrara).

Open access publishing facilitated by Universita degli Studi di Padova, as part of the Wiley - CRUI-CARE agreement.

Funding

This work was supported by the PDiSC 2024 project "EasyBackTherapy" and FAR 2023.

Conflicts of Interest

The authors declare no conflicts of interest.

Data Availability Statement

The data that supports the findings of this study are available in the supplementary material of this article.

References

1. N. Harbeck, F. Penault-Llorca, J. Cortes, et al., "Breast Cancer," *Nature Reviews. Disease Primers* 5 (2019): 66.

2. W. D. Foulkes, I. E. Smith, and J. S. Reis-Filho, "Triple-Negative Breast Cancer," *New England Journal of Medicine* 363 (2010): 1938–1948.

3. U. A. Matulonis, A. K. Sood, L. Fallowfield, B. E. Howitt, J. Sehouli, and B. Y. Karlan, "Ovarian Cancer," *Nature Reviews. Disease Primers* 2 (2016): 16061.

4. D. T. Le, J. N. Durham, K. N. Smith, et al., "Mismatch Repair Deficiency Predicts Response of Solid Tumors to PD-1 Blockade," *Science* 357 (2017): 409–413.

5. U. A. Matulonis, R. Shapira-Frommer, A. D. Santin, et al., "Antitumor Activity and Safety of Pembrolizumab in Patients with Advanced Recurrent Ovarian Cancer: Results from the Phase II KEYNOTE-100 Study," *Annals of Oncology* 30 (2019): 1080–1087.

6. S. Pignata, S. C. Cecere, A. Du Bois, P. Harter, and F. Heitz, "Treatment of Recurrent Ovarian Cancer," *Annals of Oncology* 28 (2017): 51−56.

7. L. A. Torre, B. Trabert, C. DeSantis, et al., "Ovarian Cancer Statistics," *CA: A Cancer Journal for Clinicians* 68 (2018): 284–296.

8. Y.-A. Heo, "Mirvetuximab Soravtansine: First Approval," *Drugs* 83 (2023): 265–273.

9. D. Mauricio, S. Bellone, L. Mutlu, et al., "Trastuzumab Deruxtecan (DS-8201a), a HER2-Targeting Antibody–drug Conjugate with Topoisomerase I Inhibitor Payload, Shows Antitumor Activity in Uterine and Ovarian Carcinosarcoma with HER2/Neu Expression," *Gynecologic Oncology* 170 (2023): 38–45.

10. R. Oun, Y. E. Moussa, and N. J. Wheate, "The Side Effects of Platinum-Based Chemotherapy Drugs: A Review for Chemists," *Dalton Transactions* 47 (2018): 6645–6653.

11. M. Ravera, E. Gabano, M. J. McGlinchey, and D. Osella, "Pt(Iv) Antitumor Prodrugs: Dogmas, Paradigms, and Realities," *Dalton Transactions* 51 (2021): 2121–2134.

12. T. Babu, R. P. K. Muthuramalingam, W. H. Chng, et al., "Multitargeting Pt(IV) Derivatives of Cisplatin or Oxaliplatin Inhibit Tumor Growth in Mice without Inducing Neuropathic Pain," *Journal of Medicinal Chemistry* 68 (2025): 1608–1618.

13. T. Scattolin, G. Valente, L. Luzietti, et al., "Synthesis and Anticancer Activity of Pt(0)-olefin Complexes Bearing 1,3,5-triaza-7-phosphaadamantane and *N* -heterocyclic Carbene Ligands," *Applied Organometallic Chemistry* 35 (2021): e6438.

14. N. Compagno, R. Piccolo, E. Bortolamiol, et al., "Platinum(0)-η2-1, 2-(E)ditosylethene Complexes Bearing Phosphine, Isocyanide and N-Heterocyclic Carbene Ligands: Synthesis and Cytotoxicity Towards Ovarian and Breast Cancer Cells," *Molecules* 29 (2024): 1119.

15. M. C. Dietl, M. Maag, S. Ber, et al., "Comparative Study of the Antiproliferative Activity of Heterometallic Carbene Gold(i)–platinum(Ii) and Gold(i)–palladium(Ii) Complexes in Cancer Cell Lines," *Chemical Science* 15 (2024): 15291–15298.

16. L. Ma, L. Li, and G. Zhu, "Platinum-Containing Heterometallic Complexes in Cancer Therapy: Advances and Perspectives," *Inorganic Chemistry Frontiers* 9 (2022): 2424–2453.

17. A. A. Nazarov, C. G. Hartinger, and P. J. Dyson, "Opening the Lid on Piano-Stool Complexes: An Account of ruthenium(II)–arene Complexes with Medicinal Applications," *Journal of Organometallic Chemistry* 751 (2014): 251–260.

18. M. Sojka and P. Gamez, "Exploring the Toxicity of Mononuclear Piano-Stool Ru(II) Anticancer Agents: A Comprehensive Literature Review," *Coordination Chemistry Reviews* 543 (2025): 216902.

19. C. Scolaro, A. Bergamo, L. Brescacin, et al., "In Vitro and In Vivo Evaluation of Ruthenium(II)−Arene PTA Complexes," *Journal of Medicinal Chemistry* 48 (2005): 4161–4171.

20. A. Catalano, A. Mariconda, M. S. Sinicropi, et al., "Biological Activities of Ruthenium NHC Complexes: An Update," *Antibiotics* 12 (2023): 365.

21. S. Bonnet, "Ruthenium-Based Photoactivated Chemotherapy," *Journal of the American Chemical Society* 145 (2023): 23397–23415.

22. I. Ott, "On the Medicinal Chemistry of Gold Complexes as Anticancer Drugs," *Coordination Chemistry Reviews* 253 (2009): 1670–1681.

23. G. Moreno-Alcántar, P. Picchetti, and A. Casini, "Gold Complexes in Anticancer Therapy: From New Design Principles to Particle-Based Delivery Systems," *Angewandte Chemie International Edition* 262 (2023): e202218000.

24. J. L. Hickey, R. A. Ruhayel, P. J. Barnard, M. V. Baker, S. J. Berners-Price, and A. Filipovska, "Mitochondria-Targeted Chemotherapeutics: The Rational Design of Gold(I) *N*-Heterocyclic Carbene Complexes That Are Selectively Toxic to Cancer Cells and Target Protein Selenols in Preference to Thiols," *Journal of the American Chemical Society* 130 (2008): 12570–12571.

25. E. Schlegel, Z. Papadopoulos, N. Montesdeoca, et al., "Gold(I) *N*-Heterocyclic Carbene Complexes as Ferroptosis Inducing Anticancer Agents," *ACS Medicinal Chemistry Letters* 16 (2025): 856–864.

10990682c, 0, Downloaded from https://chemistry-europe.onlinelibrary.wiley.com/doi/10.1002/ejic.70285 by Universita Di Ferrara, Wiley Online Library on [30/07/2026]. See the Terms and Conditions (https://onlinelibrary.wiley.com/terms-and-conditions) on Wiley Online Library for rules of use; OA articles are governed by the applicable Creative Commons License

26. T. Scattolin, G. Tonon, E. Botter, S. G. Guillet, N. V. Tzouras, and S. P. Nolan, "Gold(I)-*N*-Heterocyclic Carbene Synthons in Organometallic Synthesis," *Chemistry – A European Journal* 29 (2023): e202301961.

27. T. Scattolin, P. Lippmann, M. Beliš, K. Van Hecke, I. Ott, and S. P. Nolan, "A Simple Synthetic Entryway into (*N*-heterocyclic Carbene)gold-steroidyl Complexes and Their Anticancer Activity," *Applied Organometallic Chemistry* 38 (2024): e6624.

28. T. Lorenzon, Z. Papadopoulos, A. Rubbi, et al., "Synthesis of Ananikov-Type N-Heterocyclic Carbene Golden Synthons as Ferroptosis Inducing Anticancer Agents," *Inorganic Chemistry Frontiers* 13 (2026): 3986–4004, https://doi.org/10.1039/d6qi00134c.

29. N. B. Pozsoni, C. Donati, L. Rigon, et al., "Gold(i)–indomethacin Anticancer Candidates with Anti-Breast Cancer Stem Cell Properties," *Dalton Transactions* 55 (2026):5960–5969, https://doi.org/10.1039/d6dt00194g.

30. T. Scattolin, V. A. Voloshkin, F. Visentin, and S. P. Nolan, "A Critical Review of Palladium Organometallic Anticancer Agents," *Cell Reports. Physical Science* 2 (2021): 100446.

31. A. C. F. Caires, "Recent Advances Involving Palladium (II) Complexes for the Cancer Therapy," *Anti-Cancer Agents in Medicinal Chemistry* 7 (2007): 484–491.

32. T. T. Fong, C. Lok, C. Y. Chung, et al., "Cyclometalated Palladium(II) N-Heterocyclic Carbene Complexes: Anticancer Agents for Potent In Vitro Cytotoxicity and In Vivo Tumor Growth Suppression," *Angewandte Chemie International Edition* 55 (2016): 11935–11939.

33. X.-Q. Zhou, M. Xiao, V. Ramu, et al., "The Self-Assembly of a Cyclometalated Palladium Photosensitizer into Protein-Stabilized Nanorods Triggers Drug Uptake In Vitro and In Vivo," *Journal of the American Chemical Society* 142 (2020): 10383–10399.

34. G. Tonon, M. Mauceri, E. Cavarzerani, et al., "Unveiling the Promising Anticancer Activity of Palladium(Ii)–aryl Complexes Bearing Diphosphine Ligands: A Structure–activity Relationship Analysis," *Dalton Transactions* 53 (2024): 8463–8477.

35. F. Bru, M. Vanwynsberghe, E. Botter, et al., "Synthesis of Gold(I) and Palladium(II) Complexes Bearing *N* -Heterocyclic Carbene Thioglucosides with Selective Cytotoxicity Towards Ovarian Cancer Cells," *European Journal of Inorganic Chemistry* 28 (2024): e202400822.

36. E. Bortolamiol, M. Mauceri, R. Piccolo, et al., "Palladium(II)-Indenyl Complexes Bearing N-Heterocyclic Carbene (NHC) Ligands as Potent and Selective Metallodrugs toward High-Grade Serous Ovarian Cancer Models," *Journal of Medicinal Chemistry* 67 (2024): 14414–14431.

37. E. Bortolamiol, F. Fama, Z. Zhang, et al., "Cationic Palladium(Ii)-Indenyl Complexes Bearing Phosphines as Ancillary Ligands: Synthesis, and Study of Indenyl Amination and Anticancer Activity," *Dalton Transactions* 51 (2022): 11135–11151.

38. C. Donati, I. I. Hashim, N. B. Pozsoni, et al., "Investigation of the *In Vitro* Anticancer Potential of Bis(imino)acenaphthene–N-Heterocyclic Carbene Transition Metal Complexes Revealed TrxR Inhibition and Triggering of Immunogenic Cell Death (ICD) for Allyl Palladates," *RSC Medicinal Chemistry* 16 (2025): 2592–2602.

39. C. Santini, M. Pellei, V. Gandin, M. Porchia, F. Tisato, and C. Marzano, "Advances in Copper Complexes as Anticancer Agents," *Chemical Reviews* 114 (2013): 815–862.

40. S. Abdolmaleki, A. Aliabadi, and S. Khaksar, "Unveiling the Promising Anticancer Effect of Copper-Based Compounds: A Comprehensive Review," *Journal of Cancer Research and Clinical Oncology* 150 (2024): 213.

41. P. Ji, P. Wang, H. Chen, et al., "Potential of Copper and Copper Compounds for Anticancer Applications," *Pharmaceuticals* 16 (2023): 234.

42. A. Hussain, M. F. AlAjmi, Md T. Rehman, et al., "Copper(II) Complexes as Potential Anticancer and Nonsteroidal Anti-Inflammatory Agents: In Vitro and In Vivo Studies," *Scientific Reports* 9 (2019): 5237.

43. N. V. Tzouras, T. Scattolin, A. Gobbo, et al., "A Green Synthesis of Carbene-Metal-Amides (CMAs) and Carboline-Derived CMAs with Potent *in vitro* and *Ex Vivo* Anticancer Activity," *ChemMedChem* 17 (2022): e202200135.

44. H. V. Huynh, "Electronic Properties of N-Heterocyclic Carbenes and Their Experimental Determination," *Chemical Reviews* 118 (2018): 9457–9492.

45. S. Díez-González and S. P. Nolan, "Stereoelectronic Parameters Associated with N-heterocyclic Carbene (NHC) Ligands: A Quest for Understanding," *Coordination Chemistry Reviews* 251 (2006): 874–883.

46. S. Popov and H. Plenio, "Determination of Stereoelectronic Properties of NHC Ligands *via* Ion Pairing and Fluorescence Spectroscopy," *European Journal of Inorganic Chemistry* 2021 (2021): 3708–3718.

47. T. Tsang, C. I. Davis, and D. C. Brady, "Copper Biology," *Current Biology* 31 (2021): R421–R427.

48. J. Xie, Y. Yang, Y. Gao, and J. He, "Cuproptosis: Mechanisms and Links with Cancers," *Molecular Cancer* 22 (2023): 46.

49. L. Oehninger, R. Rubbiani, and I. Ott, "N-Heterocyclic Carbene Metal Complexes in Medicinal Chemistry," *Dalton Transactions* 42 (2012): 3269–3284.

50. Q. Zhao, B. Han, C. Peng, et al., "A Promising Future of Metal- *N* -heterocyclic Carbene Complexes in Medicinal Chemistry: The Emerging Bioorganometallic Antitumor Agents," *Medicinal Research Reviews* 44 (2024): 2194–2235.

51. E. Zampieri, C. Donati, V. Mechrouk, et al., "Gold(I) Complexes with NHC Ligands Functionalized with Sulfoxide Groups: Design, Synthesis, In Vitro Studies and Insights into the Mechanism of Action as Anticancer Drugs," *Journal of Inorganic Biochemistry* 271 (2025): 112957.

52. R. De Marco, V. Giuso, T. Achard, et al., "Exploring the Coordination Properties of Phosphonium-Functionalized N-Heterocyclic Carbenes Towards Gold," *European Journal of Inorganic Chemistry* 26 (2023): e202300184.

53. L. Benhamou, N. Vujkovic, V. César, H. Gornitzka, N. Lugan, and G. Lavigne, "Facile Derivatization of a "Chemo-Active" NHC Incorporating an Enolate Backbone and Relevant Tuning of Its Electronic Properties," *Organometallics* 29 (2010): 2616–2630.

54. L. Benhamou, V. César, H. Gornitzka, N. Lugan, and G. Lavigne, "Imidazol-2-Ylidene-4-Olate: an Anionic N-Heterocyclic Carbene Pre-Programmed for Further Derivatization," *Chemical Communications* (2009): 4720.

55. D. V. Pasyukov, M. A. Shevchenko, K. E. Shepelenko, et al., "One-Step Access to Heteroatom-Functionalized Imidazol(in)ium Salts," *Angewandte Chemie International Edition* 61 (2021): e202116131.

56. R. J. Griffin, "*The Medicinal Chemistry* of the Azido Group," *Progress in Medicinal Chemistry* 31 (1994): 121–232.

57. S. Bräse, C. Gil, K. Knepper, and V. Zimmermann, "Organic Azides: An Exploding Diversity of a Unique Class of Compounds," *Angewandte Chemie International Edition* 44 (2005): 5188–5240.

58. G. C. Tron, T. Pirali, R. A. Billington, P. L. Canonico, G. Sorba, and A. A. Genazzani, "Click Chemistry Reactions in Medicinal Chemistry: Applications of the 1,3-dipolar Cycloaddition between Azides and Alkynes," *Medicinal Research Reviews* 28 (2007): 278–308.

59. P. M. Levine, E. Lee, A. Greenfield, et al., "Androgen Receptor Antagonism by Divalent Ethisterone Conjugates in Castrate-Resistant Prostate Cancer Cells," *ACS Chemical Biology* 7 (2012): 1693–1701.

60. M. Huxley, C. Sanchez-Cano, M. J. Browning, et al., "An Androgenic Steroid Delivery Vector That Imparts Activity to a Non-Conventional Platinum(II) Metallo-Drug," *Dalton Transactions* 39 (2010): 11353.

10990682c, 0, Downloaded from https://chemistry-europe.onlinelibrary.wiley.com/doi/10.1002/ejic.70285 by Universita Di Ferrara, Wiley Online Library on [30/07/2026]. See the Terms and Conditions (https://onlinelibrary.wiley.com/terms-and-conditions) on Wiley Online Library for rules of use; OA articles are governed by the applicable Creative Commons License

61. E. Chardon, G. L. Puleo, G. Dahm, S. Fournel, G. Guichard, and S. Bellemin-Laponnaz, "Easy Derivatisation of Group 10 N-Heterocyclic Carbene Complexes and In Vitro Evaluation of an Anticancer Oestradiol Conjugate," *ChemPlusChem* 77 (2012): 1028–1038.

62. E. Chardon, G. L. Puleo, G. Dahm, G. Guichard, and S. Bellemin-Laponnaz, "Direct Functionalisation of Group 10 N-Heterocyclic Carbene Complexes for Diversity Enhancement," *Chemical Communications* 47 (2011): 5864.

63. J. S. Modica-Napolitano and J. R. Aprille, "Delocalized Lipophilic Cations Selectively Target the Mitochondria of Carcinoma Cells," *Advanced Drug Delivery Reviews* 49 (2001): 63–70.

64. B. R. Van Ausdall, J. L. Glass, K. M. Wiggins, A. M. Aarif, and J. Louie, "A Systematic Investigation of Factors Influencing the Decarboxylation of Imidazolium Carboxylates," *Journal of Organic Chemistry* 74 (2009): 7935–7942.

65. A. Beillard, X. Bantreil, T.-X. Métro, J. Martinez, and F. Lamaty, "Unraveling the Synthesis of Homoleptic $[Ag(N,N\text{-Diaryl-NHC})_2]Y$ ($Y = BF_4$, PF_6) Complexes by Ball-Milling," *Dalton Transactions* 45 (2016): 17859–17866.

66. T. Scattolin and S. P. Nolan, "Synthetic Routes to Late Transition Metal–NHC Complexes," *Trends in Chemistry* 2 (2020): 721–736.

67. T. Scattolin, A. A. Logvinov, N. V. Tzouras, C. S. J. Cazin, and S. P. Nolan, "Advances in the Synthesis and Applications of *N*-Heterocyclic Carbene Metal Complexes with a Focus on the Weak Base Route," *Organometallics* 42 (2023): 2692–2730.

68. D. Canseco-González, I. Rodríguez-Victoria, T. Apan-Ramírez, et al., "Facile, Single-Step Synthesis of a Series of D-Ring Ethisterones Substituted with 1,4-1,2,3-Triazoles: Preliminary Evaluation of Cytotoxic Activities," *ChemMedChem* 18 (2023): e202200659.

69. M. R. L. Furst and C. S. J. Cazin, "Copper N-Heterocyclic Carbene (NHC) Complexes as Carbene Transfer Reagents," *Chemical Communications* 46 (2010): 6924.

70. O. Santoro, A. Collado, A. M. Z. Slawin, S. P. Nolan, and C. S. J. Cazin, "A General Synthetic Route to [Cu(X)(NHC)] (NHC = N-Heterocyclic Carbene, X = Cl, Br, I) Complexes," *Chemical Communications* 49 (2013): 10483.

71. X. Ma, S. G. Guillet, M. Peng, K. Van Hecke, and S. P. Nolan, "A Simple Synthesis of $[RuCl_2$ (NHC)(*p*-Cymene)] Complexes and Their use in Olefin Oxidation Catalysis," *Dalton Transactions* 50 (2021): 3959–3965.

72. T. Achard, J. Egly, M. Sigrist, A. Maisse-François, and S. Bellemin-Laponnaz, "Easy Ruthenium-Catalysed Oxidation of Primary Amines to Nitriles under Oxidant-Free Conditions," *Chemistry – A European Journal* 25 (2019): 13271–13274.

73. M. O. Hengartner, "The Biochemistry of Apoptosis," *Nature* 407 (2000): 770–776.

74. P. Golstein and G. Kroemer, "Cell Death by Necrosis: Towards a Molecular Definition," *Trends in Biochemical Sciences* 32 (2006): 37–43.

75. G. Zhang, V. Gurtu, S. R. Kain, and G. Yan, "Early Detection of Apoptosis Using a Fluorescent Conjugate of Annexin V," *BioTechniques* 23 (1997): 525–531.

76. A. Baldisserotto, M. Demurtas, I. Lampronti, et al., "Synthesis and Evaluation of Antioxidant and Antiproliferative Activity of 2-Arylbenzimidazoles," *Bioorganic Chemistry* 94 (2019): 103396.

77. R. Barbari, C. Tupini, E. Durini, et al., "Design, Synthesis and Evaluation of New Multifunctional Benzothiazoles as Photoprotective, Antioxidant and Antiproliferative Agents," *Molecules* 28 (2022): 287.

78. R. P. Hegde, N. Demitri, A. Héroux, et al., "Macromolecular Crystallography at Elettra: Current and Future Perspectives," *Journal of Synchrotron Radiation* 32 (2025): 757–765.

79. W. Kabsch, "*XDS*," *Acta Crystallographica Section D Biological Crystallography* 66 (2010): 125–132.

80. G. M. Sheldrick, *SADABS Version 2014/5* (University of Göttingen, 2014).

81. G. M. Sheldrick, "*SHELXT* – Integrated Space-Group and Crystal-Structure Determination," *Acta Crystallographica Section A* 71 (2015): 3.

82. G. M. Sheldrick, "WinGX and ORTEP for Windows: an Update," *Acta Crystallographica Section c* 71 (2015): 3.

83. P. Emsley, B. Lohkamp, W. G. Scott, and K. Cowtan, "Features and Development of *Coot*," *Acta Crystallographica. Section D, Biological Crystallography* 66 (2010): 486–501.

84. L. J. Farrugia, "*WinGX* and *ORTEP for Windows* : an Update," *Journal of Applied Crystallography* 45 (2012): 849–854.

85. L. Schrodinger, *The PyMOL Molecular Graphics System* (Schrodinger, LLC, 2015), http://www.pymol.org.

Supporting Information

Additional supporting information can be found online in the Supporting Information section.

10990682c, 0, Downloaded from https://chemistry-europe.onlinelibrary.wiley.com/doi/10.1002/ejic.70285 by Universita Di Ferrara, Wiley Online Library on [30/07/2026]. See the Terms and Conditions (https://onlinelibrary.wiley.com/terms-and-conditions) on Wiley Online Library for rules of use; OA articles are governed by the applicable Creative Commons License